arXiv:2301.12221v1 [q-bio.CB] 28 Jan 2023

MULTISCALE MODELLING OF HEAVY METALS ADSORPTION ON ALGAL-BACTERIAL PHOTOGRANULES

F. RUSSO[1], A. TENORE[1], M.R. MATTEI[1], AND L. FRUNZO[1]

[1]Department of Mathematics and Applications "Renato Caccioppoli", University of Naples Federico II, Via Cintia 1, Montesantangelo, 80126, Naples, Italy
Corresponding author: M.R. Mattei, mariarosaria.mattei@unina.it

Abstract. A multiscale mathematical model describing the genesis and ecology of algal-bacterial photogranules and the metals biosorption on their solid matrix within a sequencing batch reactor (SBR) is presented. The granular biofilm is modelled as a spherical free boundary domain with radial symmetry and a vanishing initial value. The free boundary evolution is governed by an ordinary differential equation (ODE) accounting for microbial growth, attachment and detachment phenomena. The model is based on systems of partial differential equations (PDEs) derived from mass conservation principles. Specifically, two systems of nonlinear hyperbolic PDEs model the growth of attached species and the dynamics of free adsorption sites; and two systems of quasi-linear parabolic PDEs govern the diffusive transport and conversion of nutrients and metals. The model is completed with systems of impulsive ordinary differential equations (IDEs) describing the evolution of dissolved substrates, metals, and planktonic and detached biomasses within the granular-based SBR. All main phenomena involved in the process are considered in the mathematical model. Moreover, the dual effect of metal presence on the formation process of photogranules is accounted: metal stimulates the production of EPS by sessile species and negatively affects the metabolic activities of microbial species. To describe the effects related to metal presence, a stimulation term for EPS production and an inhibition term for metal are included in all microbial kinetics. The model is used to examine the role of the microbial species and EPS in the adsorption process, and the effect of metal concentration and adsorption proprieties of biofilm components on the metal removal. Numerical results show that the model accurately describes the photogranules evolution and ecology and confirm the applicability of algal-bacterial photogranules systems for metal-rich wastewater treatment.

1. Introduction

Increased use of metals in process industries has resulted in the production of large quantities of wastewater effluents containing high level of toxic heavy metals [1]. Due to their non-degradable and persistent nature, tendency to accumulate, and hazardous effects on living organisms and environment, heavy metals removal represents a great challenge in the wastewater treatment field [2, 1, 3, 4]. The relevance of these topics in the environmental engineering has led to the development of new technologies for heavy metals removal. Methods for removing metal ions from aqueous solutions include physical, chemical, and biological processes [5]. Nevertheless, conventional physical/chemical technologies, such as chemical precipitation, ion exchange, activated carbon adsorption and membrane processes, are often ineffective or expensive in the case of very low metals concentrations [3, 4, 6]. A promising alternative technology for removal of heavy metals from wastewater is represented by the adsorption process and, particularly, biosorption process. Indeed, compared with conventional metals removal methods, biosorption has several advantages: utilization of renewable biomaterials; possibility to treat large volumes of wastewater; high selectivity; recovery of bound heavy metals from the biomass;

no supplementation of expensive chemical reagents; low production of hazardous waste [4].

Biosorption is a complex combination of processes, consisting of the physical adherence or bonding of ions and molecules (sorbate), dissolved or suspended in a liquid phase (solvent), onto a solid surface (adsorbent) [4, 5, 7, 8, 9]. Until now, a variety of biomaterials and microorganisms have been used as biosorbent for the removal of metals, such as algae, bacteria, fungi, and yeast [4]. Such living or dead organisms are able to bind and concentrate metals, metalloids, radionuclides, and other toxic pollutants from even very dilute aqueous solutions [4, 5, 9, 10]. Several factors can affect the mechanism of metals biosorption: properties of the biomass (living or non-living, type of biomass, phenotype), presence of other competing ions, and environmental conditions (pH, temperature, etc.) [3, 4]. Specifically, the biomass phenotype may be considered one of the most important factors. Indeed, the use of freely-suspended microbial biosorbents has some disadvantages, including small particle size, low density, poor mechanical strength, low rigidity, difficulty in separating biomass and effluent, and poor biomass regeneration [4, 5, 8]. For this reason, in the recent years immobilized biomass has been regarded an interesting alternative. In addition, cell agglomeration promotes the secretion of extracellular polymeric substances (EPS), which further contribute to microorganisms protection and metals biosorption [11, 12, 13].

The simultaneous removal of organic substances and heavy metals from wastewater is still a major engineering problem. Algal-bacterial systems are expected to have a great potential in removing organic and inorganic compounds in a single treatment step, combining high adsorption capacities of microalgae and cyanobacteria with low process costs [14]. Indeed, microalgae and cyanobacteria show great tendency to produce EPS and high metal binding affinity. Moreover, the photosynthetic activity leads to the production of oxygen and allows the oxidation of carbon and nitrogen compounds by heterotrophic and nitrifying bacteria without external supplementation of oxygen [15, 16]. In this context, self-immobilized algal-bacterial consortia in granular form, known as oxygenic photogranules (OPGs), are considered as an effective and promising technology for biosorption of inorganic pollutants and degradation of organic compounds [17, 2]. In the last years, great attention has been devoted to individual removal of heavy metals [18, 19] or organic compounds [15, 20] in OPGs-based systems. Nevertheless, there is knowledge lack regarding their contextual removal, although these pollutants usually exist together in industrial wastewater.

In this framework, mathematical modelling represents a useful tool to explore the granulation process of OPGs and the metals adsorption on the matrix of biofilm granules. Biosorption is usually described through isotherms, which represent the equilibrium relationship between the adsorbate concentration in the liquid phase and the adsorbate concentration onto the adsorbent phase at a given temperature. For the adsorption of a single component, the most widely used isotherm model is the Langmuir-Freundlich model, which is the combination of Langmuir and Freundlich models [4]. Although biosorption isotherm models have been widely recognized as efficient tools to provide a suitable description of the experimental behavior, kinetic modelling is typically preferred for practical applications and process design. Pseudo-first and pseudo-second order kinetic equations are the most widely used rate equations for the adsorption process [4]. Nevertheless, more comprehensive and accurate models need to be developed to better explore the complex relationships which establish between biosorbent and sorbate. A mathematical model accounting for the biosorption process of heavy metals on the different components of a multispecies biofilm has been presented by D'Acunto et al. [7] in the case of planar biofilm.

This mono-dimensional biofilm model is conceived in the framework of continuum mathematical modeling of biofilm growth and explicitly accounts for the diffusion and adsorption of heavy metals on the biofilm matrix. Nevertheless, none of the existing models addresses the evolution and dynamics of granular biofilms formation and the adsorption processes on their solid matrix.

In this work, we propose a mathematical model to investigate the mutual interactions between the formation of oxygenic photogranules (biosorbents) and the adsorption of heavy metals (sorbates) on their solid matrix. The *de novo* granulation process of OPGs in a granular-based sequencing batch reactor (SBR) has been addressed by Tenore et al. [21]. It examines all the main factors influencing the granulation process of algal-bacterial photogranules for the treatment of typical municipal wastewater. The OPGs model has been extended to explicitly account for metals diffusion from bulk liquid to biofilm and their adsorption on the matrix of biofilm granules. Following the approach proposed by Masic and Eberl [22, 23] in the case of one-dimensional planar biofilms, the mesoscopic granular biofilm model has been coupled to the mass balances within the macroscopic bioreactor. This multiscale approach leads to model the formation and ecology of the biofilm granules and the performances of the SBR system, considering the interaction between the granules and bulk liquid. The granular biofilm model, derived in Tenore et al. [24], is formulated as a spherical free boundary value problem under the assumption of radial symmetry. Processes of microbial growth, attachment, and detachment are included to describe the formation and expansion of granules. The *de novo* granulation process is modelled by assuming that all biomass initially present in the bioreactor is in planktonic form. Mathematically, this corresponds to consider a vanishing initial value of the granule radius, using the approach introduced by D'Acunto et al. [25, 26] in the case of planar biofilm. Attachment is modelled as a continuous flux (from the bulk liquid to the biofilm) of planktonic species, which aggregate, switch their phenotype from planktonic to sessile and initiate the granulation process. Detachment is modelled as a continuous flux (from the biofilm to the bulk liquid) proportional to the square of the granule radius. The model accounts for the first time the dynamics of the detached biomass and its influence on the biological process. Specifically, detached microbial species are modelled as a new set of variables, and are supposed to grow on soluble substrates and switch to planktonic form. Furthermore, the model includes the diffusion and consumption/production of soluble substrates, due to the metabolic activity of sessile, planktonic and detached biomasses.

The model considers the adsorption of heavy metals on the granular solid matrix. Experimental observations show that each biofilm component is characterized by the presence of specific number of adsorption sites, which are able to adsorb the contaminants present in the wastewater. For this purpose, model equations describing the variation of free binding sites, and diffusion and adsorption of metals have been here derived for the first time in the case of granular biofilm, by following the approach proposed by Tenore et al. [24]. The variation of free binding sites is assumed to depend on the biofilm growth and adsorption process, and is modelled through a system of hyperbolic partial differential equations (PDEs) [7]. While, the diffusion and consumption of the sorbates is described by a system of parabolic PDEs [7].

All the main components of the OPGs are accounted in the model in sessile and suspended (planktonic and detached) form: phototrophs, facultative heterotrophic bacteria, nitrifying bacteria, EPS and inactive material (EPS and inactive material are accounted only as sessile biomass). Since cyanobacteria (included among phototrophs) play a predominant role in the granulation of oxygenic photogranules due to their filamentous morphology [15, 16, 27], phototrophs are assumed to have better attachment properties and to

enhance the attachment of other species [21]. Moreover, the model accounts the diffusion and conversion of inorganic and organic carbon, nitrate, ammonia, oxygen, and metal. The soluble substrates are involved in the metabolism of microbial species, while metal adsorbs on matrix of biofilm granules. Notably, the presence of metals in a such biological system results in a dual effect: it enhances the production of EPS by sessile species [28] and negatively affects the microbial metabolic activities [14]. This is modelled including a stimulation term for EPS production and an inhibition term for metal in all microbial kinetics. Light is included in the model to consider its effects on the metabolic activity of phototrophs. Specifically, light intensity is supposed to be constant in the bulk liquid and vary within the granules due to attenuation phenomena. Various numerical studies have been performed to investigate how the metal concentration and the adsorption properties of the biofilm components may affect the evolution of the process.

The paper is organized as follows. The mathematical model is introduced and described in Section 2, while the biological context is described in section 3. Numerical studies and results are reported in Section 4 and discussed in Section 5.

2. Mathematical Model

The mathematical model simulates the biosorption process of metals within a granular-based sequencing batch reactor (SBR) with a multiscale approach. The SBR system is modelled as a batch bioreactor having a cyclic configuration, in which N_G identical granules are immersed. For this purpose, two different biological compartments can be identified: the granule mesoscale and the bioreactor macroscale. The model is able to contextually describe the *de novo* granulation process of granular biofilms, SBR performances, and biosorption process. The interactions between the mesoscale and macroscale are accounted in the model, by considering exchange fluxes (from/to bulk liquid and to/from biofilm) of dissolved substances (substrates, products, and metals) and biomasses (in sessile and suspended form). All main phenomena involved in the *de novo* granulation process are accounted in the model: attachment process by planktonic cells; growth and decay of sessile, planktonic and detached biomasses; EPS secretion; diffusion of dissolved substrates within the granule; conversion of dissolved substrates within the granules and the bulk liquid; detachment process; conversion of detached biomass into planktonic biomass. Moreover, the biosorption process of heavy metals on granule matrix is included in the model, by considering the diffusion and bioconversion of metals, and the variation of free absorption sites.

Modelling of both the granule mesoscale and bioreactor macroscale is discussed in the following, describing the processes, assumptions, variables, equations, and initial and boundary conditions involved.

2.1. Granule mesoscale model.

The mathematical model describing the *de novo* granulation process derived by Tenore et al. [24] has been here extended to model the biosorption process of heavy metals on granular biofilms matrix. The granule mesoscale consists of a fixed number of biofilm granules (N_G) immersed within the bulk liquid and assumed to be identical at each instant. Specifically, each granule is assumed as constituted by various particulate components (including active microbial species, extracellular polymeric substances, and inactive biomass). The granules expansion depends on growth and decay processes of the various species, attachment flux from the bulk liquid to the biofilm, and detachment flux from the biofilm to the bulk liquid. The growth of microbial species depends on the presence of nutrients necessary for their metabolic activities. The nutrients are modelled as soluble substrates able to diffuse within the granules. Granulation process

is initiated by attachment of pioneering planktonic cells, while detachment phenomena lead to the loss of sessile biomass, induced by external shear forces, substrates depletion and biomass decay. Each component of the granules has a specific absorption capacity and is characterized by the presence of a certain number of free binding sites, quantified as volume fractions. The metals (sorbates) are modelled as dissolved substances, which diffuse across the granules and are subjected to absorption phenomena on the various biofilm components.

The granular biofilm is modelled as a spherical free boundary domain under the assumption of radial symmetry. The evolution of free boundary domain is described by the variation of the granule radius $R(t)$. A vanishing initial domain ($R(0) = 0$) is considered to fully model the *de novo* granulation process. The center of the granule is located at $r = 0$, where r denotes the radial coordinate. The granule model includes n microbial species in sessile form $X_i(r,t)$, m_1 dissolved substrates $S_j(r,t)$, n free binding sites $X_{\theta_i}(r,t)$, $m_2 - m_1$ heavy metals $M_j(r,t)$. All these variables are expressed in terms of concentration and modelled as functions of time t and space r. Each microbial species is supposed to have the same biomass density ρ, and the same density of binding sites ρ_θ. By dividing sessile species concentrations $X_i(r,t)$ by ρ and the free binding sites concentrations $X_{\theta_i}(r,t)$ by ρ_θ, biofilm volume fractions $f_i(r,t)$ and free binding sites volume fractions $\theta_i(r,t)$ are achieved. Notably, both $f_i(r,t)$ and $\theta_i(r,t)$ (in absence of metals adsorption) are constrained to add up to unity at each location and time ($\sum_{i=1}^{n} f_i$ and $\sum_{i=1}^{n} \theta_i$) [29].

In summary, the model components describing the granular biofilm mesoscale are:

$$X_i,\ i = 1, ..., n,\ \mathbf{X} = (X_1, ..., X_n) \tag{1}$$

$$f_i = \frac{X_i}{\rho},\ i = 1, ..., n,\ \mathbf{f} = (f_1, ..., f_n) \tag{2}$$

$$S_j,\ j = 1, ..., m_1,\ \mathbf{S} = (S_1, ..., S_{m_1}) \tag{3}$$

$$X_{\theta_i},\ i = 1, ..., n,\ \boldsymbol{X_\theta} = (X_{\theta_1}, ..., X_{\theta_n}) \tag{4}$$

$$\theta_i = \frac{X_{\theta_i}}{\rho_\theta},\ i = 1, ..., n,\ \boldsymbol{\theta} = (\theta_1, ..., \theta_n) \tag{5}$$

$$M_j,\ j = m_1 + 1, ..., m_2,\ \mathbf{M} = (M_{m_1+1}, ..., M_{m_2}) \tag{6}$$

Based on the continuum approach introduced in Wanner and Gujer [30] for one-dimensional planar biofilms, the model equations for granular biofilms were derived in Tenore et al. [24] under the assumption of radial symmetry from mass balance considerations in a differential volume of a spherical domain.

The growth and the transport of sessile species within the granular biofilm is governed by the following system of non-linear hyperbolic partial differential equations (PDEs):

$$\frac{\partial f_i(r,t)}{\partial t} + u(r,t)\frac{\partial f_i(r,t)}{\partial r} = r_{M,i}(r,t,\mathbf{f},\mathbf{S},\mathbf{M}) - f_i(r,t)\sum_{i=1}^{n} r_{M,i}(r,t,\mathbf{f},\mathbf{S},\mathbf{M}),$$
$$i = 1, ..., n, 0 \le r \le R(t),\ t > 0, \tag{7}$$

where $r_{Mi}(r,t,\mathbf{f},\mathbf{S},\mathbf{M})$ is the growth rate of the i^{th} sessile microbial species; and $u(r,t)$ is the biomass velocity.

$u(r,t)$ is governed by the following equation:

$$\frac{\partial u(r,t)}{\partial r} = -\frac{2u(r,t)}{r} + \sum_{i=1}^{n} r_{M,i}(r,t,\mathbf{f},\mathbf{S},\mathbf{M}),\ 0 < r \leq R(t),\ t > 0. \tag{8}$$

The evolution of the free boundary domain is described by the variation of the biofilm granule radius $R(t)$, according to the following equation derived from global mass balances considerations on the granule volume:

$$\dot{R}(t) = u(R(t),t) + \sigma_a(t) - \sigma_d(t). \tag{9}$$

Attachment flux is modelled as a continuous mass flux from the bulk liquid to the granule, given by the sum of the attachment fluxes $\sigma_{a,i}(t)$ of the planktonic microbial species present in the liquid phase. The term $\sigma_{a,i}(t)$ is modelled as a linear function of the concentration of the i^{th} planktonic species in the bulk liquid [25, 26]:

$$\sigma_a(t) = \sum_{i=1}^{n} \sigma_{a,i}(t) = \sum_{i=1}^{n} \frac{v_{a,i}\psi_i^*(t)}{\rho}, \tag{10}$$

where $v_{a,i}$ is the attachment velocity of the i^{th} planktonic species; and $\psi_i^*(t)$ is the concentration of the i^{th} planktonic species within the bulk liquid.

While, detachment flux is modelled as a quadratic function of the granule radius, by following the modelling approach proposed by Abbas et al. [31] for the planar case. The term $\sigma_{d,i}(t)$ is modelled as the product between the detachment flux and biofilm volume fraction of the i^{th} sessile biomass at the interface biofilm - bulk liquid:

$$\sigma_d(t) = \sum_{i=1}^{n} \sigma_{d,i}(t) = \sum_{i=1}^{n} \lambda R^2(t) f_i(R(t),t) = \lambda R^2(t), \tag{11}$$

where λ is the detachment coefficient and is supposed to be equal for all microbial species.

Attachment phenomena prevail on detachment phenomena in the initial stage of the *de novo* granulation process, while detachment phenomena become predominant as the granule dimension increases.

The diffusion and conversion of soluble substrates are governed by the following system of parabolic PDEs:

$$\begin{gathered}\frac{\partial S_j(r,t)}{\partial t} - D_{S,j}\frac{\partial^2 S_j(r,t)}{\partial r^2} - \frac{2D_{S,j}}{r}\frac{\partial S_j(r,t)}{\partial r} = r_{S,j}(r,t,\mathbf{f},\mathbf{S},\mathbf{M}),\\ j = 1,...,m_1,\ 0 < r < R(t),\ t > 0,\end{gathered} \tag{12}$$

where $r_{S,j}(r,t,\mathbf{f},\mathbf{S},\mathbf{M})$ represents the conversion rate of the j^{th} substrate; and $D_{S,j}$ denotes the diffusion coefficient in biofilm for the j^{th} dissolved substrate.

Further systems of PDEs have been derived to model the variation of free binding sites and diffusion and adsorption of metals. As in the case of sessile species, the transport of free binding sites is modelled as an advective process [7]. Thus, the model equations governing the dynamics of the free binding sites take the following form:

$$\begin{gathered}\frac{\partial X_{\theta_i}(r,t)}{\partial t} + \frac{1}{r^2}\frac{\partial}{\partial r}(r^2 u(r,t) X_{\theta_i}(r,t)) = \rho_\theta r_{\theta,i}(r,t,\boldsymbol{X}_\theta,\mathbf{M}) + \frac{\rho_\theta}{\rho}\mu_{M,i}(r,t,\mathbf{X},\mathbf{S},\mathbf{M}),\\ i = 1,...,n,\ 0 \leq r \leq R(t),\ t > 0,\end{gathered} \tag{13}$$

where $\mu_{M,i}(r,t,\mathbf{X},\mathbf{S},\mathbf{M})$ is the i^{th} specific growth rate; and $r_{\theta,i}(r,t,\boldsymbol{X}_\theta,\mathbf{M})$ is the consumption rate of the i^{th} sessile species absorption sites. The term $\frac{\rho_\theta}{\rho}\mu_{M,i}(r,t,\mathbf{X},\mathbf{S},\mathbf{M})$ accounts for the increment of free binding sites due to the sessile biomass growth; while,

their consumption is related to biosorption and decay processes, which are taken into account through $r_{\theta,i}(r,t,\boldsymbol{X}_\theta,\mathbf{M})$.

Dividing Eq.(13) by ρ_θ and considering Eq. (2) and Eq. (5) yields:

$$\frac{\partial\theta_i(r,t)}{\partial t}+\frac{1}{r^2}\frac{\partial}{\partial r}(r^2u(r,t)\theta_i(r,t))=r_{\theta,i}(r,t,\boldsymbol{\theta},\mathbf{M})+\mu_{M,i}(r,t,\mathbf{f},\mathbf{S},\mathbf{M}),\\ i=1,...,n,\ 0\le r\le R(t),\ t>0, \tag{14}$$

$$\frac{\partial\theta_i(r,t)}{\partial t}+\theta_i(r,t)\frac{\partial u(r,t)}{\partial r}+\frac{2u(r,t)\theta_i(r,t)}{r}+u(r,t)\frac{\partial\theta_i(r,t)}{\partial r}=\\ =r_{\theta,i}(r,t,\boldsymbol{\theta},\mathbf{M})+\mu_{M,i}(r,t,\mathbf{f},\mathbf{S},\mathbf{M}),\\ i=1,...,n,\ 0\le r\le R(t),\ t>0. \tag{15}$$

Substituting Eq.(8) into Eq.(15) yields:

$$\frac{\partial\theta_i(r,t)}{\partial t}+u(r,t)\frac{\partial\theta_i(r,t)}{\partial r}=\\ r_{\theta,i}(r,t,\boldsymbol{\theta},\mathbf{M})+\mu_{M,i}(r,t,\mathbf{f},\mathbf{S},\mathbf{M})-\theta_i(r,t)\sum_{i=1}^{n}r_{M,i}(r,t,\mathbf{f},\mathbf{S},\mathbf{M}),\\ i=1,...,n,\ 0\le r\le R(t),\ t>0, \tag{16}$$

As for soluble substrates, the transport of dissolved heavy metals is modelled as a diffusive process [7], and it is expressed as follows:

$$\frac{\partial M_j(r,t)}{\partial t}-D_{M,j}\frac{\partial^2M_j(r,t)}{\partial r^2}-\frac{2D_{M,j}}{r}\frac{\partial M_j(r,t)}{\partial r}=r_{A,j}(r,t,\boldsymbol{\theta},\mathbf{M}),\\ j=m_1+1,...,m_2,\ 0<r<R(t),\ t>0, \tag{17}$$

where $r_{A,j}(r,t,\boldsymbol{\theta},\mathbf{M})$ and $D_{M,j}$ denote the adsorption rate and diffusion coefficient of the j^{th} dissolved metal within the biofilm.

2.2. **Bioreactor macroscale model.** The reactor macroscale is modelled as a sequencing batch reactor in which N_G granules having the same properties are immersed. Specifically, the reactor is characterized by the presence of a number of soluble substrates involved in the biological process and heavy metals taking part in the biosorption process. Besides the sessile biomass (granules), also planktonic and detached biomasses are considered in the bulk liquid. Planktonic species contribute to the genesis of the granules, while detached biomass is formed as a result of the detachment process. The modelling choice to include planktonic and detached biomass as two different variables derives from the experimental experience that the newly detached biomass has different properties from both sessile and planktonic biomass [32, 33, 34]. Both planktonic and detached biomasses (suspended biomasses) contribute to the conversion of soluble substrates in the bulk liquid. Reconversion of detached biomass into planktonic biomass is also modelled. The bioreactor model is formulated for n microbial species in planktonic form $\psi_i^*(t)$, n microbial species deriving from the detachment process $\psi_{d_i}^*(t)$, m_1 dissolved substrates $S_j^*(t)$, and m_2-m_1 heavy metals $M_j^*(t)$. All these variables are expressed in terms of concentration and modelled as functions of time and not of space, since the reactor is modeled as a completely mixed reactor. An SBR is based on a sequence of treatment cycles constituted by four phases:

- filling phase, in which the reactor is fed with a fixed volume of wastewater;
- reaction phase, in which the wastewater volume is biologically treated through the biomass present in the system;

- settling phase, which consists in the solid-liquid separation;
- emptying phase, in which the clarified supernatant is partially removed from the reactor.

The filling, settling and emptying phases are supposed to be instantaneous, and the duration of the reaction phase is supposed to be the same as the cycle duration. 100% settling efficiency is assumed for biofilm granules, while the suspended biomass has a partial settling efficiency. Moreover, since the volume occupied by the biomass in granular and suspended form is neglected, the reactor volume is assumed to be the same as the liquid volume. The cyclic configuration of the SBR is modelled with a system of first order impulsive ordinary differential equations (IDEs) [21, 35]. An IDE is described by three components: the continuous-time differential equation, which governs the state of the system between impulses; the impulse equation, which describes an impulsive jump and is defined by a jump function at the instant the impulse occurs; and the jump criterion, which defines a set of jump events in which the impulse equation is active.

In summary, the model components describing the bulk liquid are:

$$\psi_i^*,\ i=1,...,n,\ \boldsymbol{\psi}^*=(\psi_1^*,...,\psi_n^*), \tag{18}$$

$$\psi_{d_i}^*,\ i=1,...,n,\ \boldsymbol{\psi_d^*}=(\psi_{d_1}^*,...,\psi_{d_n}^*), \tag{19}$$

$$S_j^*,\ j=1,...,m_1,\ \mathbf{S}^*=(S_1^*,...,S_{m_1}^*), \tag{20}$$

$$M_j^*,\ j=m_1+1,...,m_2,\ \mathbf{M}^*=(M_{m_1+1}^*,...,M_{m_2}^*), \tag{21}$$

while, the system of IDEs is the following:

$$\begin{gathered}V\dot{\psi}_i^*(t)=-\sigma_{a,i}(t)\rho A(t)N_G+Vr_{\psi,i}^*(t,\boldsymbol{\psi}^*,\mathbf{S}^*,\mathbf{M}^*)+Vr_{C,i}^*(t,\boldsymbol{\psi}_d^*),\\ t\in[0,T],\ t\neq t_k, i=1,...,n\ \ t>0,\end{gathered} \tag{22}$$

$$\begin{gathered}V\dot{\psi}_{d_i}^*(t)=\sigma_{d,i}(t)\rho A(t)N_G+Vr_{\psi_d,i}^*(t,\boldsymbol{\psi}_d^*,\mathbf{S}^*,\mathbf{M}^*)-Vr_{C,i}^*(t,\boldsymbol{\psi}_d^*),\\ t\in[0,T],\ t\neq t_k, i=1,...,n\ \ t>0,\end{gathered} \tag{23}$$

$$\begin{gathered}V\dot{S}_j^*(t)=-A(t)N_GD_{S,j}\frac{\partial S_j(R(t),t)}{\partial r}+Vr_{S,j}^*(t,\boldsymbol{\psi}^*,\boldsymbol{\psi}_d^*,\mathbf{S}^*,\mathbf{M}^*),\\ t\in[0,T],\ t\neq t_k,\ j=1,...,m_1,\ \ t>0,\end{gathered} \tag{24}$$

$$\begin{gathered}V\dot{M}_j^*(t)=-A(t)N_GD_{M,j}\frac{\partial M_j(R(t),t)}{\partial r},\\ t\in[0,T],\ t\neq t_k, j=m_1+1,...,m_2,\ \ t>0,\end{gathered} \tag{25}$$

where V is the volume of the bulk liquid; $A(t)$ is the area of the spherical granule and is equal to $4\pi R^2(t)$; $r_{\psi,i}^*(t,\boldsymbol{\psi}^*,\mathbf{S}^*,\mathbf{M}^*)$ and $r_{\psi_d,i}^*(t,\boldsymbol{\psi}_d^*,\mathbf{S}^*,\mathbf{M}^*)$ are the growth rates for the i^{th} planktonic and detached biomass, respectively; $r_{S,j}^*(t,\boldsymbol{\psi}^*,\boldsymbol{\psi}_d^*,\mathbf{S}^*,\mathbf{M}^*)$ is the conversion rate for the j^{th} soluble substrates; and $r_{C,i}^*(t,\boldsymbol{\psi}_d^*)$ is the reconversion rate of the i^{th} detached biomasses into planktonic form.

The jump functions associated to Eqs. (22)-(25) are:

$$\Delta\psi_i^*(t_k)=\psi_i^*(t_k^+)-\psi_i^*(t_k^-)=-\gamma\psi_i^*(t_k^-),\ k=1,...,h,\ i=1,...,n, \tag{26}$$

$$\Delta\psi_{d_i}^*(t_k)=\psi_{d_i}^*(t_k^+)-\psi_{d_i}^*(t_k^-)=-\gamma\psi_{d_i}^*(t_k^-),\ k=1,...,h,\ i=1,...,n, \tag{27}$$

$$\Delta S_j^*(t_k) = S_j^*(t_k^+) - S_j^*(t_k^-) = -\omega S_j^*(t_k^-) + \omega S_j^{in},\ k = 1, ..., h,\ j = 1, ..., m_1, \tag{28}$$

$$\Delta M_j^*(t_k) = M_j^*(t_k^+) - M_j^*(t_k^-) = -\omega M_j^*(t_k^-) + \omega M_j^{in},\ k = 1, ..., h,\ j = m_1+1, ..., m_2, \tag{29}$$

where γ is the fraction of suspended biomass removed during the emptying phase; ω is the emptying/refilling ratio; S_j^{in} and M_j^{in} are the concentrations of the j^{th} substrate and j^{th} metal in the influent; $0 = t_0 < t_1 < ... < t_h < t_{h+1} = T$, $t_{k+1} - t_k = \tau$; τ is the duration of the cycle; $\psi_i^*(t_k^+)$, $\psi_{d_i}^*(t_k^+)$, $S_j^*(t_k^+)$, $M_j^*(t_k^+)$, $\psi_i^*(t_k^-)$,$\psi_{d_i}^*(t_k^-)$, $S_j^*(t_k^-)$, and $M_j^*(t_k^-)$ are the right and left limits of ψ_i^*, $\psi_{d_i}^*$, S_j^* and M_j^* at time t_k.

Such systems of IDEs are derived from mass balance considerations and describe the dynamics of planktonic and detached biomasses, soluble substrates, and heavy metals within the bulk liquid. Equation (22) represents the mass balance of the i^{th} microbial species in planktonic form. In particular, the mass variation over time within the bioreactor (first member) is due to the exchange flux related to the attachment process (first term of the second member), the metabolic activity in the bulk liquid (second term of the second member), and the conversion of the detached biomass into planktonic form (third term of the second member). Similarly, Eq. (23) represents the mass balance of the i^{th} detached microbial species. In particular, the mass variation over time within the bioreactor (first member) is due to the exchange flux related to the detachment process (first term of the second member), the metabolic activity in the bulk liquid (second term of the second member), and the conversion of the detached biomass into planktonic form (third term of the second member). Obviously, the attachment flux represents a negative contribution for the planktonic biomasses, while the detachment process is a positive contribution for the detached biomasses. The conversion rate from detached to planktonic state causes two opposite contributions: positive in the equation of planktonic species and negative in the equation of detached biomasses. Eq. (24) represents the mass balance of the j^{th} soluble substrate. In this case, the mass variation over time within the bioreactor (first member) is due to the exchange flux between the bulk liquid and the granular biofilms related to the diffusion phenomenon (first term of the second member) and its consumption and/or production occurring in the bulk liquid and mediated by the planktonic and detached biomasses (second term of second member). Lastly, Eq. (25) represents the mass balance of the j^{th} dissolved metal. In this case, the mass variation over time within the bioreactor (first member) is due to only the exchange flux between the bulk liquid and the granular biofilms related to the diffusion phenomenon. Indeed, its consumption in the bulk liquid mediated by the planktonic and detached biomasses is neglected.

2.3. **Initial and boundary conditions.** To integrate Eqs. (7)-(9), (12), (16), (17), (22)-(25), it is necessary to specify initial and boundary conditions. The *de novo* granulation process is modelled by coupling a vanishing initial condition to Eq. (9):

$$R(0) = 0. \tag{30}$$

The boundary condition for Eq. (8) is given by:

$$u(0, t) = 0,\ t > 0. \tag{31}$$

The granule radius $R(t)$ represents the free boundary of the mathematical problem. Its variation, governed by Eq. (9), depends on attachment σ_a and detachment σ_d velocity. In the initial phase, the granule radius is small and, consequently, attachment prevails on detachment. Therefore, it is $\sigma_a - \sigma_d > 0$ and the free boundary is a space-like line. During

maturation, the granule dimension increases, and the detachment is the prevailing process. Thus, it is $\sigma_a - \sigma_d < 0$, and the free boundary is a time-like line. When the free boundary is a space-like line, there is a mass flux from bulk liquid to granule, and the biofilm volume fractions at the granule-bulk liquid interface are dependent on characteristics of the bulk liquid. In particular, the volume fractions of sessile biomass depend on the concentration of planktonic biomass in the bulk liquid:

$$f_i(R(t),t) = \frac{v_{a,i}\psi_i^*(t)}{\sum_{i=1}^{n} v_{a,i}\psi_i^*(t)},\ i = 1,...,n,\ t > 0,\ \sigma_a(t) - \sigma_d(t) > 0, \tag{32}$$

while, the volume fractions of the free binding sites are fixed equal to the biofilm volume fractions at the granule-bulk liquid interface:

$$\theta_i(R(t),t) = f_i(R(t),t),\ i = 1,...,n,\ t > 0,\ \sigma_a(t) - \sigma_d(t) > 0. \tag{33}$$

When the free boundary is a time-like line, there is a mass flux from the granule to the bulk liquid. Thus, the volume fractions at the interface are regulated exclusively by the internal points of the biofilm domain and conditions (32) and (33) are not required.

For what concerns substrates and metals diffusion (Eq. (12) and Eq. (17)), a no flux condition is fixed at the granule center ($r = 0$), and a Dirichlet condition is considered at the granule-bulk liquid interface ($r = R(t)$):

$$\frac{\partial S_j}{\partial r}(0,t) = 0,\ S_j(R(t),t)) = S_j^*(t),\ j = 1,...,m_1,\ t > 0, \tag{34}$$

$$\frac{\partial M_j}{\partial r}(0,t) = 0,\ M_j(R(t),t)) = M_j^*(t),\ j = m_1+1,...,m_2,\ t > 0, \tag{35}$$

Note that $S_j^*(t)$ and $M_j^*(t)$ are the solutions of Eq. (24) and Eq. (25), respectively.

Eqs. (7), (12), (16), and (17) refer to the biofilm domain and do not require initial conditions, since the extension of the biofilm domain is zero at $t = 0$.

Lastly, the following initial conditions are considered for Eqs. (22)-(25):

$$\psi_i^*(0) = \psi_{i,0}^*,\ i = 1,...,n, \tag{36}$$

$$\psi_{d_i}^*(0) = \psi_{d_{i,0}}^*,\ i = 1,...,n, \tag{37}$$

$$S_j^*(0) = S_{j,0}^*,\ j = 1,...,m_1, \tag{38}$$

$$M_j^*(0) = M_{j,0}^*,\ j = m_1+1,...,m_2, \tag{39}$$

where $\psi_{i,0}^*$, $\psi_{d_i,0}^*$, $S_{j,0}^*$, and $M_{j,0}^*$ are the initial concentrations of the i^{th} planktonic and detached biomass, and the j^{th} soluble substrate and dissolved metal within the bulk liquid, respectively.

3. Biochemical framework: OPGs granulation and adsorption processes

The mathematical model described above simulates the biosorption process of metals on the matrix of biofilm granules, occurring in a granular-based SBR system, and is able to contextually describe granules genesis and ecology, bioreactor performances, and adsorption process of inorganic compounds. In this work, the model is applied to study the ecology of OPGs and the adsorption process of a generic metal on their solid matrix.

3.1. **Metabolic kinetics of OPGs.** All main biological processes involved in the OPGs lifecycle are included in the mathematical model. For this purpose, phototrophs PH, heterotrophic bacteria H, and nitrifying bacteria N are taken into account as active microbial species. While, the following soluble substrates are considered: inorganic carbon IC, organic carbon DOC, nitrate NO_3, ammonia NH_3, and dissolved oxygen O_2.

The growth metabolism of phototrophs is affected by light. Two different processes of phototrophic growth in presence of light are taken into account, based on the available nitrogen source. In presence of NH_3, phototrophs carry out photosynthesis, consuming IC and NH_3 and producing O_2 and DOC. In absence or shortage of ammonia, phototrophs can grow by using NO_3 as nitrogen source. Furthermore, the model takes into account the inhibition induced by the presence of O_2 on the photosynthetic activity. In absence of light, DOC, O_2, and NH_3 are consumed by the phototrophs, which produce IC. Heterotrophic bacteria use DOC as a source of carbon and energy, and produce inorganic carbon IC. They are assumed to grow under aerobic condition directly using O_2, as well as anoxic condition using NO_3 as oxygen source (denitrification process). As in the previous case, this aspect is modelled using an inhibition term for oxygen in the nitrate-based heterotrophic growth kinetic [36]. Nitrifying bacteria include ammonia-oxidizing bacteria and nitrite-oxidizing bacteria. For this reason, they are responsible for NH_3 conversion into NO_2, and the subsequent NO_2 conversion into NO_3. The same biological processes are supposed to occur in the bulk liquid, where planktonic and detached biomasses consume or produce the j^{th} soluble substrate. The mathematical model considers the production of EPS and inactive material only in sessile form. Indeed, the EPS production by suspended biomass has been neglected because it is much lower than sessile production [21], as well as the production of suspended inactive biomass that does not play any role in the biological process. Moreover, phototrophs are regarded as the main EPS contributors [28], and this aspect has been considered in the model by adopting different values of EPS fraction produced by the microbial species.

3.2. **Adsorption process.** Compared to conventional physical/chemical technologies, biosorption is effective and less expensive when the metal concentration is less than 100 $mg\ L^{-1}$ [2, 1, 3, 4, 6]. Both living and dead (metabolically inactive) biological materials are able to adsorb toxic heavy metals, as various functional groups are found on their cell wall offering strong attraction forces for the metal ions and providing high metal removal efficiency [4]. Specifically, extracellular substances produced by microorganisms have a crucial role in biosorption of metals [13] and are considered the major potential agents in biosorption processes [28]. In metal-stressed conditions microorganisms are induced to produce a higher amount of EPS, increasing the adsorption potential of the microbial consortium [28, 37]. Moreover, microorganisms not only regulate the synthesis of EPS in response to toxic elements, but also increase EPS adsorption capacities [28]. These aspects are included in the model by adopting a higher adsorption constant for EPS and considering a stimulation term for EPS production in all microbial kinetics. Also phototrophs and inactive material play an important role in adsorption processes, as they show high metals removal efficiency and can achieve more effective biosorption of metals than bacteria and fungi [37]. Indeed, metal accumulation capacity of phototrophs is comparable or sometimes higher than chemical sorbents [38], and, in addition, as mentioned before they are the main EPS producers [28]. The use of dead biomass could be a preferred alternative, as it offers high metals adsorption capacity, easy recovery of biosorbed metals, absence of toxicity limitations and nutrients requirements for growth [4, 5]. However, in the case in which the solvent consists of industrial wastewater rich in metals, organic and nitrogen compounds, the problem related to the nutrients requirement

is overcome and the utilization of algal-bacterial biomass allows to combine the advantages of EPS, microalgae and inactive material. Lastly, metals adsorption by suspended biomasses is neglected. Indeed, populations of planktonic and biofilm cells adsorb metals in different ways [39], and it is experimentally proved that immobilized bacterial cells have much higher biosorption capacities than suspended cells [40]. Moreover, the use of freely-suspended microbial biosorbents has further disadvantages including small particle size, low density, poor mechanical strength, and little rigidity, while the use of biofilms minimize these disadvantages [5].

3.3. **Modelling of heavy metals adsorption on OPGs.** In summary, the following variables are included in the model:

- Granule variables:
  - Five sessile microbial species: phototrophs $f_{PH}(r,t)$, heterotrophic bacteria $f_H(r,t)$, nitrifying bacteria $f_N(r,t)$, EPS $f_{EPS}(r,t)$, and inactive biomass $f_I(r,t)$.
  - Five soluble compounds: inorganic carbon $S_{IC}(r,t)$, organic carbon $S_{DOC}(r,t)$, nitrate $S_{NO_3}(r,t)$, ammonia $S_{NH_3}(r,t)$, and dissolved oxygen $S_{O_2}(r,t)$.
  - Five fractions of free binding sites related to: phototrophs $\theta_{PH}(r,t)$, heterotrophic bacteria $\theta_H(r,t)$, nitrifying bacteria $\theta_N(r,t)$, EPS $\theta_{EPS}(r,t)$, and inactive biomass $\theta_I(r,t)$.
  - One metal: $M(r,t)$.
- SBR variables:
  - Three planktonic microbial species: phototrophs $\psi^*_{PH}(t)$, heterotrophic bacteria $\psi^*_H(t)$, and nitrifying bacteria $\psi^*_N(t)$.
  - Three microbial species deriving from biofilm detachment: phototrophs $\psi^*_{d_{PH}}(t)$, heterotrophic bacteria $\psi^*_{d_H}(t)$, and nitrifying bacteria $\psi^*_{d_N}(t)$.
  - Five soluble compounds: inorganic carbon $S^*_{IC}(t)$, organic carbon $S^*_{DOC}(t)$, nitrate $S^*_{NO_3}(t)$, ammonia $S^*_{NH_3}(t)$, and dissolved oxygen $S^*_{O_2}(t)$.
  - One metal: $M^*(t)$

In order to account the light dependency of the phototrophic metabolism, light intensity is included as a model variable: $I(r,t)$. I is assumed to be a piecewise-constant function in the bioreactor to simulate the day-night cycle, while it varies across the granule radius due to attenuation phenomena, according to the Lambert-Beer law:

$$I(r,t) = I_0 e^{-k_{tot}(R(t)-r)\rho}, 0 \leq r \leq R(t),\ t > 0, \tag{40}$$

where I_0 is the light intensity in the bioreactor and k_{tot} is the light attenuation coefficient [41]. Also the negative effect of photoinhibition is accounted in the model [21]. Indeed, excess light can photoinhibit and slow down photosynthesis activity of phototrophs [42]. In accordance with [43], such phenomena is modelled by using the following optimum type expression:

$$\phi_I(r,t) = \frac{I(r,t)}{I_{opt}}\ e^{1-\frac{I(r,t)}{I_{opt}}},\ 0 \leq r \leq R(t),\ t > 0, \tag{41}$$

where I_{opt} is the optimum light intensity for phototrophs.

The OPGs granulation process is governed by phototrophs, in planktonic form which are able to aggregate and enclose non-phototrophic biomass in a rigid and spherical structure thanks to their filamentous morphology [15, 20]. As proposed by Tenore et al. [21], this aspect is taken into account assuming that the attachment velocities of heterotrophic and

nitrifying bacteria are functions of the planktonic phototrophs concentration within the bioreactor:

$$\sigma_{a,i}(t) = \frac{v_{a,i}\psi_i^*(t)}{\rho},\ i \in \{PH, H, N\}, \tag{42}$$

$$v_{a,i} = v_{a,i}^0,\ i \in \{PH\}, \tag{43}$$

$$v_{a,i}(\psi_{PH}^*(t)) = \frac{v_{a,i}^0\psi_{PH}^*(t)}{K_{PH} + \psi_{PH}^*(t)},\ i \in \{H, N\}, \tag{44}$$

where $v_{a,i}^0$ is the maximum attachment velocity of the i^{th} suspended species and K_{PH} is the cyanobacteria half saturation constant on the attachment of heterotrophs and nitrifiers.

All reaction terms of the model are reported below. The sessile biomasses growth rates $r_{M,i}$ and conversion rates for soluble substrates within the biofilm $r_{S,j}$, reported in Eq. (7), Eq. (8), and Eq. (12) are modelled as follows:

$$r_{M,i} = \sum_k \alpha_{i,k}\ \nu_k,\ i \in \{PH, H, N, EPS, I\},\ k = 1, ..., m, \tag{45}$$

$$r_{S,j} = \sum_k \beta_{j,k}\ \nu_k,\ j \in \{IC, DOC, NO_3, NH_3, O_2\},\ k = 1, ..., m, \tag{46}$$

where m denotes the number of biological processes occurring in the biofilm and accounted in the mathematical model; $\alpha_{i,k}$ is the stoichiometric coefficient of the i^{th} biofilm component referred to the k^{th} biological process within the biofilm (Table 1); $\beta_{j,k}$ is the stoichiometric coefficient of the j^{th} soluble substrate referred to the k^{th} biological process within the biofilm (Table 2); ν_k represents the kinetic rate of the k^{th} biological process within the biofilm (Table 3). Moreover, the conversion rates of planktonic biomasses $r_{\psi,j}^*$, detached biomasses $r_{\psi_{d_i}}^*$ and soluble substrates $r_{S,j}^*$ within the bulk liquid, reported in Eqs. (22)-(24) are defined as:

$$r_{\psi,i}^* = \sum_k \alpha_{i,k}^*\ \nu_k^*,\ i \in \{PH, H, N\},\ k = 1, ..., m, \tag{47}$$

$$r_{\psi_{d_i}}^* = \sum_k \bar{\alpha}_{i,k}^*\ \nu_k^*,\ i \in \{PH, H, N\},\ k = 1, ..., m, \tag{48}$$

$$r_{S,j}^* = \sum_k \beta_{j,k}^*\ \nu_k^*,\ j \in \{IC, DOC, NO_3, NH_3\},\ k = 1, ..., m, \tag{49}$$

$$r_{S,j}^* = \sum_k \beta_{j,k}^*\ \nu_k^* + k_{La}(S_{j,sat} - S_j^*),\ j \in \{O_2\},\ k = 1, ..., m, \tag{50}$$

where m denotes the number of biological processes occurring in the bulk liquid and accounted in the mathematical model; k_{La} and $S_{O_2,sat}$ are the oxygen mass transfer coefficient and the oxygen saturation concentration in the bulk liquid, respectively; $\alpha_{i,k}^*$ is the stoichiometric coefficient of the i^{th} planktonic species referred to the k^{th} biological process within the bulk liquid (Table 4); $\bar{\alpha}_{i,k}^*$ is the stoichiometric coefficient of the i^{th} detached species referred to the k^{th} biological process within the bulk liquid (Table 4); $\beta_{j,k}^*$ is the stoichiometric coefficient of the j^{th} soluble substrate referred for the k^{th} biological process within the bulk liquid (Table 5); ν_k^* represents the kinetic rate of the k^{th} biological process within the bulk liquid (Table 6).

Detached biomass has different characteristics from both sessile and planktonic biomasses [32, 33, 34]. Experimental observations suggest that the surface properties of detached cells clearly differ from those of planktonic and sessile cells for at least the first 48 h after detachment [33]. For this reason, the reconversion rate of the i^{th} detached species into planktonic form, reported in Eq. (22) and Eq. (23), is modelled as follows:

$$r^*_{C,i} = K_C \psi^*_{d_i}(t), \tag{51}$$

where K_C is the conversion constant from detached to planktonic form.

Regarding the adsorption process, the consumption rate of the free binding sites $r_{\theta,i}$ and the specific growth rate of sessile species $\mu_{M,i}$ in Eq. (16), and the adsorption rate of the dissolved metal r_A in Eq. (17) are listed below:

$$r_{\theta,i} = -(k_{ads,i} M + k_{d,i})\theta_i, \ i \in \{PH, H, N, EPS, I\}, \tag{52}$$

$$\mu_{M,i} = \sum_k \alpha_{i,k} \ \nu_k, \ i \in \{PH, H, N, EPS, I\}, \ k = 1, ..., \bar{m}, \tag{53}$$

$$r_A = -Y_{ads,i} \rho_\theta k_{ads,i} M \theta_i, \ i \in \{PH, H, N, EPS, I\}, \tag{54}$$

where $\bar{m}$ denotes the number of growth processes occurring in the biofilm and accounted in the mathematical model; $k_{d,i}$ is the decay-inactivation rate for the i^{th} microbial species; $Y_{ads,i}$ and $k_{ads,i}$ represent the biosorption yield and the adsorption kinetic constant of the i^{th} microbial species; ρ_θ is the density of the binding sites.

As mentioned above, in metal-stressed conditions microorganisms regulate the synthesis of EPS and are induced to produce more. To include this aspect in the model, EPS fraction produced by each the microbial species is modelled as function of the metal concentration:

$$K_{EPS,i} = \tilde{K}_{EPS,i} \left(1 + \frac{M}{K_{s,i} + M}\right), \tag{55}$$

where $\tilde{K}_{EPS,i}$ and $K_{s,i}$ are the EPS fraction produced by the i^{th} microbial species in absence of toxic pollutants and the stimulation constant for EPS of the i^{th} microbial species. The model takes into account also the toxic effect of metals on microbial metabolic processes, by considering an inhibition term in all microbial kinetics:

$$I_M = \frac{K^{in}_M}{K^{in}_M + M}, \tag{56}$$

where K^{in}_M is the inhibition coefficient for the generic heavy metal.

The values used for all stoichiometric and kinetic parameters are reported in Table 7.

	$\mathbf{x_{PH}}$	$\mathbf{x_H}$	$\mathbf{x_N}$	$\mathbf{x_{EPS}}$	$\mathbf{x_I}$	**Rate**
1	$1-k_{EPS,PH}$			$k_{EPS,PH}$		ν_1
2	$1-k_{EPS,PH}$			$k_{EPS,PH}$		ν_2
3	$1-k_{EPS,PH}$			$k_{EPS,PH}$		ν_3
4		$1-k_{EPS,H}$		$k_{EPS,H}$		ν_4
5		$1-k_{EPS,H}$		$k_{EPS,H}$		ν_5
6			$1-k_{EPS,N}$	$k_{EPS,N}$		ν_6
7	-1				1	ν_7
8		-1			1	ν_8
9			-1		1	ν_9

TABLE 1. Biochemical rate coefficients ($\alpha_{i,k}$) of the biological processes within the biofilm.

	$\mathbf{S_{IC}}$	$\mathbf{S_{DOC}}$	$\mathbf{S_{NO_3}}$	$\mathbf{S_{NH_3}}$	$\mathbf{S_{O_2}}$	**Rate**
1	$-\frac{k_{EPS,PH}+(1-k_{EPS,PH})(k_{DOC}+1.0025)}{32}$	$k_{DOC}(1-k_{EPS,PH})$	$-\frac{0.1704}{32}(1-k_{EPS,PH})$		$\frac{k_{EPS,PH}+(1-k_{EPS,PH})(k_{DOC}+1)}{32}$	ν_1
2	$-\frac{k_{EPS,PH}+(1-k_{EPS,PH})(k_{DOC}+1.0025)}{32}$	$k_{DOC}(1-k_{EPS,PH})$		$-\frac{0.1704}{32}(1-k_{EPS,PH})$	$\frac{k_{EPS,PH}+(1-k_{EPS,PH})(k_{DOC}+1.3409)}{32}$	ν_2
3	$\frac{1-1.0025\ Y_{DOC}}{32\ Y_{DOC}}$	$-\frac{1}{Y_{DOC}}$		$-\frac{0.1704}{32\ Y_{DOC}}$	$-\frac{1-Y_{DOC}}{32\ Y_{DOC}}$	ν_3
4	$\frac{1}{32\ Y_H}-0.02976$	$-\frac{1}{Y_H}$		$-\frac{0.2}{33.6}$	$-\frac{1}{32\ Y_H}+0.03125$	ν_4
5	$\frac{1}{32\ Y_H}-0.02976$	$-\frac{1}{Y_H}$	$-\frac{0.8}{32\ Y_H}+0.02857$	$-\frac{0.2}{33.6}$		ν_5
6	$-\frac{1}{33.6}$		$\frac{1}{14\ Y_N}$	$-(0.00593+\frac{1}{14\ Y_N})$	$-\frac{1}{7\ Y_N}+\frac{1}{32}$	ν_6
7						ν_7
8						ν_8
9						ν_9

TABLE 2. Biochemical rate coefficients ($\beta_{j,k}$) of the biological processes within the biofilm.

	Process	**Kinetic rate expression**
1	Growth of PH on NO_3	$\nu_1 = \mu_{max,PH} \frac{S_{IC}}{K_{PH,IC}+S_{IC}} \frac{S_{NO_3}}{K_{PH,NO_3}+S_{NO_3}} \frac{K_{PH,NH_3}}{K_{PH,NH_3}+S_{NH_3}} \frac{K^{in}_{PH,O_2}}{K^{in}_{PH,O_2}+S_{O_2}} \frac{K^{in}_M}{K^{in}_M+M} \frac{I}{I_{opt}} e^{(1-(\frac{I}{I_{opt}})} f_{PH}$
2	Growth of PH on NH_3	$\nu_2 = \mu_{max,PH} \frac{S_{IC}}{K_{PH,IC}+S_{IC}} \frac{S_{NH_3}}{K_{PH,NH_3}+S_{NH_3}} \frac{K^{in}_{PH,O_2}}{K^{in}_{PH,O_2}+S_{O_2}} \frac{K^{in}_M}{K^{in}_M+M} \frac{I}{I_{opt}} e^{(1-(\frac{I}{I_{opt}})} f_{PH}$
3	Heterotrophic growth of PH	$\nu_3 = \mu^{resp}_{max,PH} \frac{S_{DOC}}{K_{PH,DOC}+S_{DOC}} \frac{S_{O_2}}{K_{PH,O_2}+S_{O_2}} \frac{K^{in}_{PH,I}}{K^{in}_{PH,I}+I} \frac{K^{in}_M}{K^{in}_M+M} f_{PH}$
4	Aerobic growth of H	$\nu_4 = \mu_{max,H} \frac{S_{DOC}}{K_{H,DOC}+S_{DOC}} \frac{S_{NH_3}}{K_{H,NH_3}+S_{NH_3}} \frac{S_{O_2}}{K_{H,O_2}+S_{O_2}} \frac{K^{in}_M}{K^{in}_M+M} f_H$
5	Anoxic growth of H	$\nu_5 = \mu_{max,H} \frac{S_{DOC}}{K_{H,DOC}+S_{DOC}} \frac{S_{NO_3}}{K_{H,NO_3}+S_{NO_3}} \frac{S_{NH_3}}{K_{H,NH_3}+S_{NH_3}} \frac{K_{H,O_2}}{K_{H,O_2}+S_{O_2}} \frac{K^{in}_M}{K^{in}_M+M} f_H$
6	Growth of N	$\nu_6 = \mu_{max,N} \frac{S_{IC}}{K_{N,IC}+S_{IC}} \frac{S_{NH_3}}{K_{H,NH_3}+S_{NH_3}} \frac{S_{O_2}}{K_{H,O_2}+S_{O_2}} \frac{K^{in}_M}{K^{in}_M+M} f_N$
7	Death of PH	$\nu_7 = k_{d,PH} f_{PH}$
8	Death of H	$\nu_8 = k_{d,H} f_H$
9	Death of N	$\nu_9 = k_{d,N} f_N$

where $K^{in}_{PH,O_2} = K^{in}_{O_2,max} \frac{\frac{S_{IC}}{S_{O_2}}}{\frac{S_{IC}}{S_{O_2}}+K_{R_{IC/O_2}}}$

TABLE 3. Kinetic rate expressions (ν_k) of the biological processes within the biofilm.

	$\psi^*_{\mathbf{PH}}$	$\psi^*_{\mathbf{H}}$	$\psi^*_{\mathbf{N}}$	$\psi^*_{\mathbf{d_{PH}}}$	$\psi^*_{\mathbf{d_H}}$	$\psi^*_{\mathbf{d_N}}$	**Rate**
1	1						ν^*_1
2	1						ν^*_2
3	1						ν^*_3
4		1					ν^*_4
5		1					ν^*_5
6			1				ν^*_6
7				1			ν^*_7
8				1			ν^*_8
9				1			ν^*_9
10					1		ν^*_{10}
11					1		ν^*_{11}
12						1	ν^*_{12}
13	-1						ν^*_{13}
14		-1					ν^*_{14}
15			-1				ν^*_{15}
16				-1			ν^*_{16}
17					-1		ν^*_{17}
18						-1	ν^*_{18}

TABLE 4. Biochemical rate coefficients ($\alpha^*_{i,k}$ and $\bar{\alpha}^*_{i,k}$) of the biological processes within the bulk liquid.

	$\mathbf{S^*_{IC}}$	$\mathbf{S^*_{DOC}}$	$\mathbf{S^*_{NO_3}}$	$\mathbf{S^*_{NH_3}}$	$\mathbf{S^*_{O_2}}$	**Rate**
1	$-\frac{k_{DOC}+1.0025}{32}$	k_{DOC}	$-\frac{0.1704}{32}$		$\frac{k_{DOC}+1}{32}$	ν^*_1
2	$-\frac{k_{DOC}+1.0025}{32}$	k_{DOC}		$-\frac{0.1704}{32}$	$\frac{k_{DOC}+1.3409}{32}$	ν^*_2
3	$\frac{1-1.0025\ Y_{DOC}}{32\ Y_{DOC}}$	$-\frac{1}{Y_{DOC}}$		$-\frac{0.1704}{32\ Y_{DOC}}$	$-\frac{1-Y_{DOC}}{32\ Y_{DOC}}$	ν^*_3
4	$\frac{1}{32\ Y_H} - 0.02976$	$-\frac{1}{Y_H}$		$-\frac{0.2}{33.6}$	$-\frac{1}{32\ Y_H} + 0.03125$	ν^*_4
5	$\frac{1}{32\ Y_H} - 0.02976$	$-\frac{1}{Y_H}$	$-\frac{0.8}{32\ Y_H} + 0.02857$	$-\frac{0.2}{33.6}$		ν^*_5
6	$-\frac{1}{33.6}$		$\frac{1}{14\ Y_N}$	$-(0.00593 + \frac{1}{14\ Y_N})$	$-\frac{1}{7\ Y_N} + \frac{1}{32}$	ν^*_6
7	$-\frac{k_{DOC}+1.0025}{32}$	k_{DOC}	$-\frac{0.1704}{32}$		$\frac{k_{DOC}+1}{32}$	ν^*_7
8	$-\frac{k_{DOC}+1.0025}{32}$	k_{DOC}		$-\frac{0.1704}{32}$	$\frac{k_{DOC}+1.3409}{32}$	ν^*_8
9	$\frac{1-1.0025\ Y_{DOC}}{32\ Y_{DOC}}$	$-\frac{1}{Y_{DOC}}$		$-\frac{0.1704}{32\ Y_{DOC}}$	$-\frac{1-Y_{DOC}}{32\ Y_{DOC}}$	ν^*_9
10	$\frac{1}{32\ Y_H} - 0.02976$	$-\frac{1}{Y_H}$		$-\frac{0.2}{33.6}$	$-\frac{1}{32\ Y_H} + 0.03125$	ν^*_{10}
11	$\frac{1}{32\ Y_H} - 0.02976$	$-\frac{1}{Y_H}$	$-\frac{0.8}{32\ Y_H} + 0.02857$	$-\frac{0.2}{33.6}$		ν^*_{11}
12	$-\frac{1}{33.6}$		$\frac{1}{14\ Y_N}$	$-(0.00593 + \frac{1}{14\ Y_N})$	$-\frac{1}{7\ Y_N} + \frac{1}{32}$	ν^*_{12}
13						ν^*_{13}
14						ν^*_{14}
15						ν^*_{15}
16						ν^*_{16}
17						ν^*_{17}
18						ν^*_{18}

TABLE 5. Biochemical rate coefficients ($\beta^*_{i,k}$) of the biological processes within the bulk liquid.

	Process	Kinetic rate expression
1	Growth of PH on NO_3	$\nu_1^* = \mu_{max,PH} \frac{S_{IC}^*}{K_{PH,IC}+S_{IC}^*} \frac{S_{NO_3}^*}{K_{PH,NO_3}+S_{NO_3}^*} \frac{K_{PH,NH_3}}{K_{PH,NH_3}+S_{NH_3}^*} \frac{K_{PH,O_2}^{in,*}}{K_{PH,O_2}^{in,*}+S_{O_2}^*} \frac{K_{M^*}^{in}}{K_M^{in}+M^*} \frac{I_0}{I_{opt}} e^{(1-\frac{I_0}{I_{opt}})} \psi_{PH}^*$
2	Growth of PH on NH_3	$\nu_2^* = \mu_{max,PH} \frac{S_{IC}^*}{K_{PH,IC}+S_{IC}^*} \frac{S_{NH_3}^*}{K_{PH,NH_3}+S_{NH_3}^*} \frac{K_{PH,O_2}^{in,*}}{K_{PH,O_2}^{in,*}+S_{O_2}^*} \frac{K_{M^*}^{in}}{K_M^{in}+M^*} \frac{I_0}{I_{opt,PH}} e^{(1-\frac{I_0}{I_{opt}})} \psi_{PH}^*$
3	Heterotrophic growth of PH	$\nu_3^* = \mu_{max,PH}^{resp} \frac{S_{DOC}^*}{K_{PH,DOC}+S_{DOC}^*} \frac{S_{O_2}^*}{K_{PH,O_2}+S_{O_2}^*} \frac{K_{PH,I}^{in}}{K_{PH,I}^{in}+I_0} \frac{K_{M^*}^{in}}{K_M^{in}+M^*} \psi_{PH}^*$
4	Aerobic growth of H	$\nu_4^* = \mu_{max,H} \frac{S_{DOC}^*}{K_{H,DOC}+S_{DOC}^*} \frac{S_{NH_3}^*}{K_{H,NH_3}+S_{NH_3}^*} \frac{S_{O_2}^*}{K_{H,O_2}+S_{O_2}^*} \frac{K_{M^*}^{in}}{K_M^{in}+M^*} \psi_H^*$
5	Anoxic growth of H	$\nu_5^* = \mu_{max,H} \frac{S_{DOC}^*}{K_{H,DOC}+S_{DOC}^*} \frac{S_{NO_3}^*}{K_{H,NO_3}+S_{NO_3}^*} \frac{S_{NH_3}^*}{K_{H,NH_3}+S_{NH_3}^*} \frac{K_{H,O_2}}{K_{H,O_2}+S_{O_2}^*} \frac{K_{M^*}^{in}}{K_M^{in}+M^*} \psi_H^*$
6	Growth of N	$\nu_6 = \mu_{max,N}^* \frac{S_{IC}^*}{K_{N,IC}+S_{IC}^*} \frac{S_{NH_3}^*}{K_{H,NH_3}+S_{NH_3}^*} \frac{S_{O_2}^*}{K_{H,O_2}+S_{O_2}^*} \frac{K_{M^*}^{in}}{K_M^{in}+M^*} \psi_N^*$
7	Growth of PH_d on NO_3	$\nu_7^* = \mu_{max,PH} \frac{S_{IC}^*}{K_{PH,IC}+S_{IC}^*} \frac{S_{NO_3}^*}{K_{PH,NO_3}+S_{NO_3}^*} \frac{K_{PH,NH_3}}{K_{PH,NH_3}+S_{NH_3}^*} \frac{K_{PH,O_2}^{in,*}}{K_{PH,O_2}^{in,*}+S_{O_2}^*} \frac{K_{M^*}^{in}}{K_M^{in}+M^*} \frac{I_0}{I_{opt}} e^{(1-\frac{I_0}{I_{opt}})} \psi_{d_{PH}}^*$
8	Growth of PH_d on NH_3	$\nu_8^* = \mu_{max,PH} \frac{S_{IC}^*}{K_{PH,IC}+S_{IC}^*} \frac{S_{NH_3}^*}{K_{PH,NH_3}+S_{NH_3}^*} \frac{K_{PH,O_2}^{in,*}}{K_{PH,O_2}^{in,*}+S_{O_2}^*} \frac{K_{M^*}^{in}}{K_M^{in}+M^*} \frac{I_0}{I_{opt,PH}} e^{(1-\frac{I_0}{I_{opt}})} \psi_{d_{PH}}^*$
9	Heterotrophic growth of PH_d	$\nu_9^* = \mu_{max,PH}^{resp} \frac{S_{DOC}^*}{K_{PH,DOC}+S_{DOC}^*} \frac{S_{O_2}^*}{K_{PH,O_2}+S_{O_2}^*} \frac{K_{PH,I}^{in}}{K_{PH,I}^{in}+I_0} \frac{K_{M^*}^{in}}{K_M^{in}+M^*} \psi_{d_{PH}}^*$
10	Aerobic growth of H_d	$\nu_{10}^* = \mu_{max,H} \frac{S_{DOC}^*}{K_{H,DOC}+S_{DOC}^*} \frac{S_{NH_3}^*}{K_{H,NH_3}+S_{NH_3}^*} \frac{S_{O_2}^*}{K_{H,O_2}+S_{O_2}^*} \frac{K_{M^*}^{in}}{K_M^{in}+M^*} \psi_{d_H}^*$
11	Anoxic growth of H_d	$\nu_{11}^* = \mu_{max,H} \frac{S_{DOC}^*}{K_{H,DOC}+S_{DOC}^*} \frac{S_{NO_3}^*}{K_{H,NO_3}+S_{NO_3}^*} \frac{S_{NH_3}^*}{K_{H,NH_3}+S_{NH_3}^*} \frac{K_{H,O_2}}{K_{H,O_2}+S_{O_2}^*} \frac{K_{M^*}^{in}}{K_M^{in}+M^*} \psi_{d_H}^*$
12	Growth of N_d	$\nu_{12}^* = \mu_{max,N}^* \frac{S_{IC}^*}{K_{N,IC}+S_{IC}^*} \frac{S_{NH_3}^*}{K_{H,NH_3}+S_{NH_3}^*} \frac{S_{O_2}^*}{K_{H,O_2}+S_{O_2}^*} \frac{K_{M^*}^{in}}{K_M^{in}+M^*} \psi_{d_N}^*$
13	Death of PH	$\nu_{13}^* = k_{d,PH} \psi_{PH}^*$
14	Death of H	$\nu_{14}^* = k_{d,H} \psi_H^*$
15	Death of N	$\nu_{15}^* = k_{d,N} \psi_N^*$
16	Death of PH_d	$\nu_{16}^* = k_{d,PH} \psi_{d_{PH}}^*$
17	Death of H_d	$\nu_{17}^* = k_{d,H} + \psi_{d_H}^*$
18	Death of N_d	$\nu_{18}^* = k_{d,N} \psi_{d_N}^*$

where $K_{PH,O_2}^{in,*} = K_{O_2,max}^{in} \frac{\frac{S_{IC}^*}{S_{O_2}^*}}{\frac{S_{IC}^*}{S_{O_2}^*}+K_{R_{IC/O_2}}}$

TABLE 6. Kinetic rate expressions (ν_k^*) of the biological processes within the bulk liquid.

Parameter	Definition	Unit	Value	Ref
$\mu_{max,PH}$	Maximum specific growth rate for PH	d^{-1}	2.368	[36]
$\mu^{resp}_{max,PH}$	Maximum specific growth rate for PH respiration	d^{-1}	0.237	[36]
$\mu_{max,H}$	Maximum specific growth rate for H	d^{-1}	4.8	[44]
$\mu_{max,N}$	Maximum specific growth rate for N	d^{-1}	1	[44]
$k_{d,PH}$	Decay-inactivation rate for PH	d^{-1}	0.1	[36]
$k_{d,H}$	Decay-inactivation rate for H	d^{-1}	0.1	[36]
$k_{d,N}$	Decay-inactivation rate for N	d^{-1}	0.1	[36]
$K_{PH,IC}$	IC half saturation coeff. for PH	$kmol(IC)\ m^{-3}$	10^{-4}	[36]
$K_{PH,DOC}$	DOC half saturation coeff. for PH	$kg(COD)\ m^{-3}$	$5 \cdot 10^{-3}$	[36]
K_{PH,NO_3}	NO_3 half saturation coeff. for PH	$kmol(NO_3)\ m^{-3}$	$1.2 \cdot 10^{-6}$	[36]
K_{PH,NH_3}	NH_3 half saturation coeff. for PH	$kmol(NH_3)\ m^{-3}$	$1.2 \cdot 10^{-6}$	[36]
K_{PH,O_2}	O_2 half saturation coeff. for PH	$kmol(O_2)\ m^{-3}$	$3 \cdot 10^{-4}$	[36]
$K^{in}_{PH,I}$	Light inhibition coefficient for PH	$kmol(e^-)\ m^{-2}\ d^{-1}$	$8 \cdot 10^{-5}$	[36]
$K_{H,DOC}$	DOC half saturation coeff. for H	$kg(COD)\ m^{-3}$	$4 \cdot 10^{-3}$	[36]
K_{H,NO_3}	NO_3 half saturation coeff. for H	$kmol(NO_3)\ m^{-3}$	$3.6 \cdot 10^{-5}$	[36]
K_{H,NH_3}	NH_3 half saturation coeff. for H	$kmol(NH_3)\ m^{-3}$	$3.6 \cdot 10^{-6}$	[45]
K_{H,O_2}	O_2 half saturation coeff. for H	$kmol(O_2)\ m^{-3}$	$6.25 \cdot 10^{-6}$	[36]
$K_{N,IC}$	IC half saturation coeff. for N	$kmol(IC)\ m^{-3}$	10^{-4}	[36]
K_{N,NH_3}	NH_3 half saturation coeff. for N	$kmol(NH_3)\ m^{-3}$	$7 \cdot 10^{-5}$	[36]
K_{N,O_2}	O_2 half saturation coeff. for N	$kmol(O_2)\ m^{-3}$	$1.56 \cdot 10^{-5}$	[36]
$K^{in}_{O_2,max}$	Max inhibition coefficient of O_2 on PH	$kmol(O_2)\ m^{-3}$	10^{-3}	[46]
$K_{R_{IC/O_2}}$	Half saturation coeff. for O_2 inhibition	$--$	0.35	[46]
K^{in}_M	Inhibition coefficient of M	$kg(M)\ m^{-3}$	0.1	(a)
Y_H	Yield of H on DOC	$kg(COD)\ kg(COD)^{-1}$	0.63	[36]
Y_N	Yield of N on NO_3	$kg(COD)\ kg(NO_3 - N)^{-1}$	0.24	[36]
Y_{DOC}	Yield of PH on DOC	$kg(COD)\ kg(COD)^{-1}$	0.5	(a)
$\tilde{k}_{EPS,PH}$	EPS fraction produced by PH	$--$	0.23	(a)
$\tilde{k}_{EPS,H}$	EPS fraction produced by H	$--$	0.18	[47]
$\tilde{k}_{EPS,N}$	EPS fraction produced by N	$--$	0.075	[47]
k_{DOC}	DOC release fraction by PH	$--$	0.05	[41]
k_{La}	O_2 mass transfer coefficient	d^{-1}	23.3	[44]
$S_{O_2,sat}$	O_2 saturation concentration in bulk liquid	$kmol(O_2)\ m^{-3}$	$2.4 \cdot 10^{-4}$	[44]
I_{opt}	Optimum light intensity for PH	$kmol(e^-)\ m^{-2}\ d^{-1}$	0.01728	[48]
I_0	Incident light intensity in the reactor	$kmol(e^-)\ m^{-2}\ d^{-1}$	0.008	[21]
k_{tot}	Light attenuation coefficient	$m^2\ kg^{-1}$	210	[36]
$k_{ads,PH}$	Sorption constant of PH	$m^3\ kg(M)^{-1}\ d^{-1}$	$1 \cdot 10^3$	(a)
$k_{ads,H}$	Sorption constant of H	$m^3\ kg(M)^{-1}\ d^{-1}$	$2 \cdot 10^1$	(a)
$k_{ads,N}$	Sorption constant of N	$m^3\ kg(M)^{-1}\ d^{-1}$	$2 \cdot 10^1$	(a)
$k_{ads,EPS}$	Sorption constant of EPS	$m^3\ kg(M)^{-1}\ d^{-1}$	$2 \cdot 10^3$	(a)
$k_{ads,I}$	Sorption constant of I	$m^3\ kg(M)^{-1}\ d^{-1}$	$2 \cdot 10^2$	(a)
$K_{s,i}$	Stimulation constant for EPS	$kg(M)\ m^{-3}$	0.05	(a)
$Y_{ads,i}$	Yield of M on i^{th} microbial species	$kg(M)\ N^{\circ -1}_{sites}$	1	(a)
$D_{S,IC}$	Diffusion coefficient of IC in biofilm	$m^2\ d^{-1}$	$1.32 \cdot 10^{-4}$	[36]
$D_{S,DOC}$	Diffusion coefficient of DOC in biofilm	$m^2\ d^{-1}$	$0.83 \cdot 10^{-4}$	[30]
D_{S,NO_3}	Diffusion coefficient of NO_3 in biofilm	$m^2\ d^{-1}$	$1.18 \cdot 10^{-4}$	[36]
D_{S,NH_3}	Diffusion coefficient of NH_3 in biofilm	$m^2\ d^{-1}$	$1.49 \cdot 10^{-4}$	[30]
D_{S,O_2}	Diffusion coefficient of O_2 in biofilm	$m^2\ d^{-1}$	$1.75 \cdot 10^{-4}$	[30]
$D_{S,M}$	Diffusion coefficient of metal in biofilm	$m^2\ d^{-1}$	$6.05 \cdot 10^{-5}$	[49]
$v^0_{a,PH}$	Attachment velocity of ψ^*_{PH}	$m\ d^{-1}$	$3 \cdot 10^{-3}$	(a)
$v^0_{a,H}$	Attachment velocity of ψ^*_H	$m\ d^{-1}$	$5 \cdot 10^{-4}$	(a)
$v^0_{a,N}$	Attachment velocity of ψ^*_N	$m\ d^{-1}$	$5 \cdot 10^{-4}$	(a)
K_{PH}	Half saturation coeff. of ψ^*_{PH} on ψ^*_H, ψ^*_N attachment	$kg(COD)\ m^{-3}$	$3 \cdot 10^{-2}$	(a)
K_C	Conversion coeff. from detached to planktonic form	d^{-1}	0.5	(a)
ρ	Biofilm density	$kg(COD)\ m^{-3}$	37	[44]
ρ_θ	Binding sites density	$N^\circ_{sites}\ m^{-3}$	20	(a)
λ	Constant detachment coefficient	$m^{-1}\ d^{-1}$	40	(a)
V	Reactor volume	m^3	400	(a)
N_G	Number of granules in the reactor	$--$	$2.4 \cdot 10^{10}$	(a)
τ	Duration of the cycle	d	0.25	(a)
γ	Fraction of suspended biomass lost in the emptying	$--$	0.2	(a)
ω	Emptying/refilling ratio	$--$	0.5	(a)
t_{light}	Time of light condition	d	0.125	(a)
t_{dark}	Time of dark condition	d	0.125	(a)

(a) Assumed

TABLE 7. Kinetic, stoichiometric and operating parameters used for numerical simulations.

4. Numerical studies and results

The model has been integrated numerically by developing an original code in MatLab platform. Hyperbolic PDEs (7) and (16) have been integrated by using the method of characteristics, applied for the first time in the planar biofilm context by D'Acunto and Frunzo (2011) [50]. The method of lines has been used to solve the diffusion-reaction PDEs (12) and (17). The ODEs for ψ_i^*, $\psi_{d_i}^*$, S_j^*, and M_j^* (Eqs. (22)-(25)) have been integrated by using the MatLab routine ode45. Numerical simulations have been performed to investigate the genesis and evolution of oxygenic photogranules, the microbial species stratification and interaction between the functional trophic groups, and to study the SBR performances in terms of substrates removal and metal adsorption. Specifically, the first study ($SET1$) investigates the treatment process of a typical industrial wastewater containing a low concentration of a generic metal. Both the granules ecology and the process evolution have been investigated, focusing on metal effects on biofilm formation and its removal process. The second study ($SET2$) investigates how the metal concentration affects the OPGs formation and adsorption processes in terms of microbial growth and removal efficiency. Finally, the third study ($SET3$) explores the role of the adsorption capacities of all the microbial species in the adsorption process.

The wastewater influent is supposed to be fed discontinuously in the SBR. As mentioned before, in each cycle the reactor is filled with a fixed volume V of wastewater, and the substrates are biologically degraded in batch conditions. The bioreactor volume V is assumed constant and equal to 400 m^3. The number of granules N_G has been selected through an iterative procedure varying the detachment coefficient λ [24], with the aim to obtain a 25% filling ratio by considering granules with a steady-state radius of about 1 mm (an average size representative of OPGs [16, 27]). After the reaction phase, the solid-liquid separation occurs in the reactor, whereby perfect settling has been considered for granules (no granule is removed from the reactor during the emptying phase). While the fraction of suspended biomass lost during the emptying phase has been set equal to 20%. At the end of each cycle the reactor is only partially emptied and refilled with a new liquid volume to be treated (emptying/refilling ratio $\omega = 50\%$). As explained above, the reaction phase is supposed to be the same as the duration of the cycle τ, and it consists of 3 hours of darkness and 3 hours of light ($t_{dark} = t_{light} = 0.125\ d$ and $\tau = 0.25\ d$) [21, 27]. In the light phase, the reactor is supposed to be homogeneously illuminated and the incident light intensity I_0 is fixed at 0.008 $kmol\ m^{-2}\ d^{-1}$ [21].

The same wastewater influent composition is considered for each treatment cycle. It is characterized by $S_{IC}^{in} = 180\ g\ m^{-3}$ (inorganic carbon), $S_{DOC}^{in} = 500\ g\ m^{-3}$ (organic carbon), $S_{NH_3}^{in} = 50\ g\ m^{-3}$ (ammonia), $S_{NO_3}^{in} = 0$ (nitrate), $S_{O_2}^{in} = 0$ (oxygen). Such concentrations reflect the typical wastewater [51] and are usually used in experimental works [18]. The concentration of the heavy metal in the influent M^{in} is varied in the numerical studies, and its values will be provided below, case to case. The initial concentrations of soluble substrates $S_{j,0}^*$ and metal M_0^* in the bulk liquid have been set equal to the concentration within the wastewater influent (S_j^{in} and M^{in}). On the contrary, no suspended biomass is supposed to be present in the influent ($\psi_i^{in} = 0$ and $\psi_{d_i}^{in} = 0$), while phototrophic inoculum of suspended phototrophs is considered, where planktonic heterotrophic and nitrifying bacteria are present in smaller amounts: $\psi_{PH,0}^* = 600\ g\ m^{-3}$, $\psi_{H,0}^* = \psi_{N,0}^* = 50\ g\ m^{-3}$ [21]. The initial concentration of detached species $\psi_{d_i,0}^*$ in the bulk liquid has been set equal to zero ($\psi_{d_i,0}^* = 0$). Note that no addition of oxygen is considered ($S_{O_2}^{in} = 0$), since it is provided by photosynthesis of phototrophs.

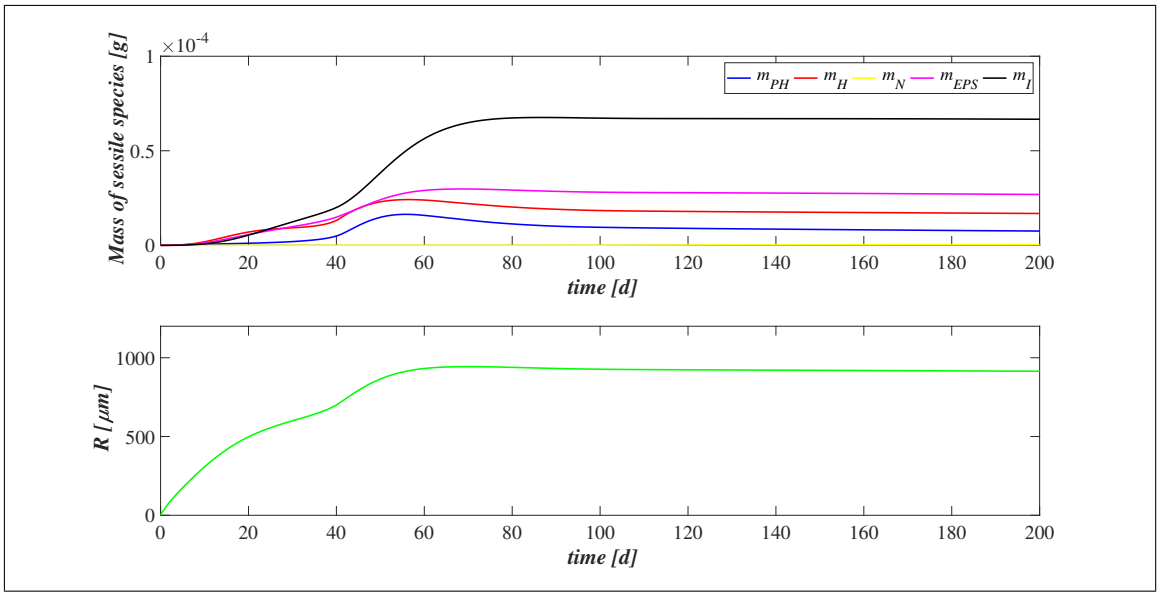


FIGURE 1. $SET1$ - Evolution of biofilm radius and mass of sessile species over time. Wastewater influent composition: $S_{IC}^{in} = 180\ g\ m^{-3}$ (inorganic carbon), $S_{DOC}^{in} = 500\ g\ m^{-3}$ (organic carbon), $S_{NH_3}^{in} = 50\ g\ m^{-3}$ (ammonia), $S_{NO_3}^{in} = 0$ (nitrate), $S_{O_2}^{in} = 0$ (oxygen), $M^{in} = 100\ g\ m^{-3}$ (metal). Incident light intensity: $I_0 = 0.008\ kmol\ m^{-2}\ d^{-1}$. Duration of the cycle: $\tau = 6\ h$. Time of light exposure: $t_{light} = 50\%\ \tau$.

Since the phototrophs are the major EPS producers in algal-bacterial biofilm, their EPS fraction produced in absence of toxic pollutants is assumed to be higher than heterotrophs ($\tilde{K}_{EPS,H} = 0.18$ [47]) and nitrifiers ($\tilde{K}_{EPS,N} = 0.075$ [47]) and is fixed at $\tilde{K}_{EPS,PH} = 0.23$. Such value is within the range of typical EPS fraction values of phototrophic biomass [36]. Regarding the adsorption kinetic constants of the biofilm components, $k_{ads,EPS}$, $k_{ads,PH}$ and $k_{ads,I}$ are supposed to be much higher than $k_{ads,H}$ and $k_{ads,N}$, since the adsorption process is predominantly governed by EPS, phototrophs and inactive material. Finally, as mentioned above, attachment velocity of phototrophs is assumed to be a constant value and it is set equal to the average value of attachment velocities of microalgae and cyanobacteria used by Tenore et al. [21]. All parameters used in this model are reported in Table 7.

The simulation time T is fixed to 200 d for all simulations. This time interval guarantees to achieve the steady-state configuration in terms of: performance of SBR cycles (including soluble substrates S_j^*, metal M^*, planktonic species ψ_i^*, and detached biomasses $\psi_{d_i}^*$), granule size $R(t)$; microbial composition and distribution within the granules (in terms of fraction f_i and mass m_i); volume fractions of free binding sites θ_i; and concentration of free metal M within the biofilm.

4.1. **SET1 - Evaluation of metal removal from industrial wastewater in OPGs-based system.** The first set $SET1$ describes the treatment process of a typical industrial wastewater with a low concentration of metal ($M^{in} = 100\ g\ m^{-3}$), occurring in a granular-based sequencing batch reactor (simulation $S1$). The microbial stratification of oxygenic photogranules, nutrients degradation, and metal adsorption are investigated. The $SET1$ results are shown in Figs. 1-4.

Fig. 1 reports the evolution of the overall mass of sessile species $m_i(t)$ (top) and photogranule radius $R(t)$ (bottom) over time. The active sessile biomasses constituting the biofilm matrix (phototrophs, heterotrophs and nitrifiers) grow by converting the nutrients, and decay producing inert material. Such biomasses can interact with each other, cooperating and/or competing. In presence of light, phototrophs produce O_2 and DOC consuming IC and NH_3 (or NO_3), and consequently they promote the heterotrophs and nitrifiers growth. Indeed, heterotrophic bacteria require O_2 (or NO_3 in anoxic condition) and DOC for their metabolic activities. While NH_3 and O_2 are necessary for nitrifying bacteria, which compete with phototrophs for IC. However, nitrifiers produce NO_3 necessary for heterotrophs in anoxic condition and for phototrophs in lack or shortage of NH_3. Under dark conditions, phototrophs compete with heterotrophs and nitrifiers for O_2 and with all heterotrophs for DOC. In return, heterotrophic bacteria produce IC necessary for the metabolism of phototrophs in light conditions and nitrifiers. In the initial days, the intense attachment process leads to the formation of photogranules mainly composed by phototrophs. Oxygen production during the photosynthesis promotes the growth of heterotrophic bacteria. Thus, the heterotrophic biomass rapidly increases with respect to the other microbial species, thanks to their high growth rates in presence of elevate availability of DOC. It should be noted that the metabolism of all biomasses is initially inhibited, due to the presence of free metal. In this phase the photogranule slowly increases, achieving a radius of about 600 μm (Fig. 1 - bottom). After 40 days, when a relevant amount of metal is already adsorbed on biofilm matrix, a more rapid phototrophs (blue) growth is observed. As consequence, heterotrophs (red) metabolism and production of EPS (magenta) and inert material (black) are favoured. This, in turn, leads to a faster increase of the granule radius. Subsequently, the detachment process becomes more relevant and limits the granule expansion leading to a steady-state dimension of about 920 μm. A very low mass of nitrifying bacteria (yellow) is observed throughout the process, because they have lower maximum growth rates than heterotrophic bacteria which are more competitive in the use of O_2 in presence of DOC.

Fig. 2 shows the microbial stratification within the granule (from first row to fourth row) and the free metal concentration (fifth row) at different times. After 20 and 30 days, significant fractions of phototrophs (blue) and heterotrophs (red) can be observed throughout the granule. Indeed, phototrophs are responsible for the genesis of the photogranules due to their granulation properties, while heterotrophic bacteria have the highest growth rate. Obviously, in the initial stage of the process the concentration of free metal (black) is still elevate and the metal diffuses throughout the granule inhibiting the microorganisms growth. Passing from $T = 30$ d to $T = 40$ d the concentration of free metal significantly reduces thanks to the growth of phototrophs (see Fig. 4). Indeed, phototrophs have a tendency to secrete EPS higher than other microbial species, and both phototrophs and EPS have higher adsorption capabilities than heterotrophs and nitrifiers. Thanks to the metal consumption, phototrophs are in turn less inhibited and continue to grow. The steady-state of microbial species distribution and free metal concentration is achieved at $T = 80$ d. Note that phototrophs and EPS are present in relevant amounts and a clear microbial species stratification can be observed: phototrophic biomass accumulates in the outermost layers, where optimal light conditions are guaranteed; heterotrophic bacteria predominantly populate the external part of the granule; EPS (magenta) is homogeneously distributed throughout the granule. In addition, as observed in Fig. 1, nitrifying bacteria (yellow) are almost absent. As regard the free metal diffusion, after the complete evolution of the granule, the adsorption process is completed, and a gradient of free metal

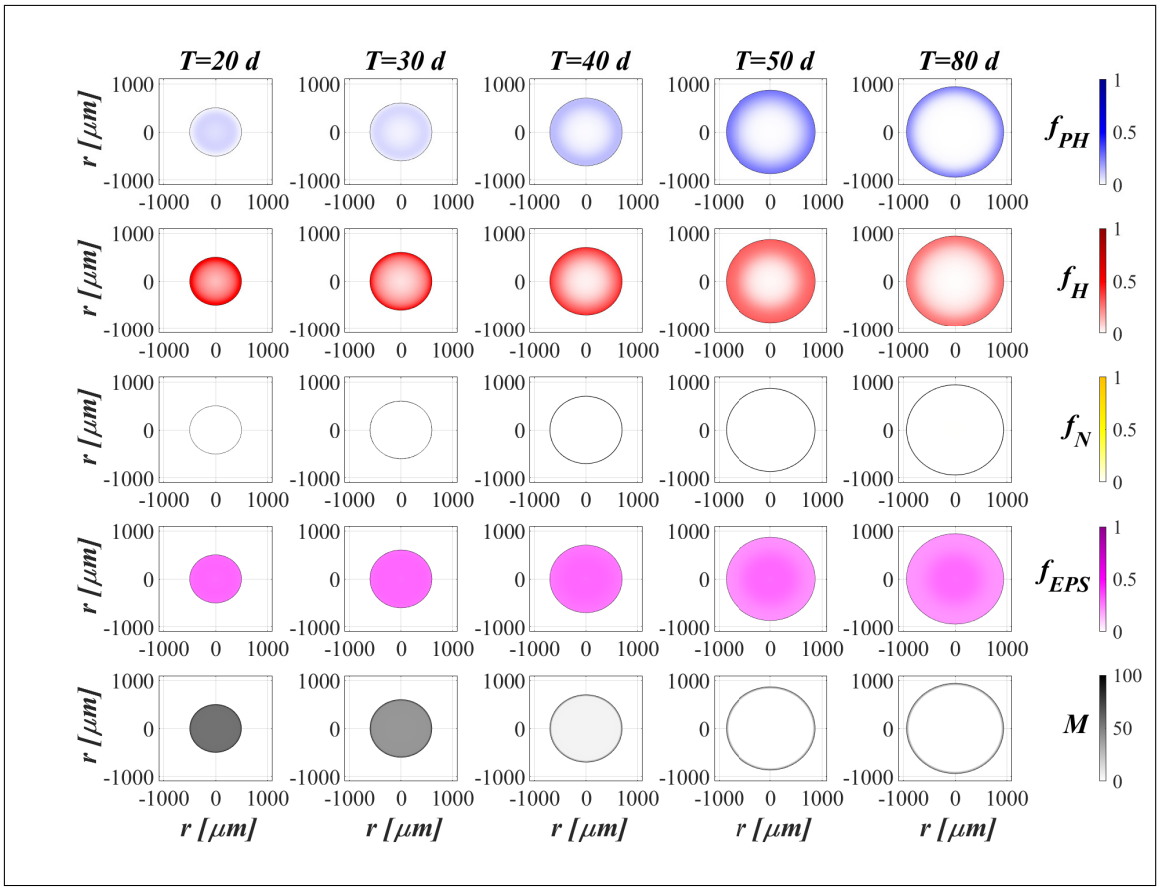


FIGURE 2. $SET1$- Active microbial species distribution and concentration of free metal within the diametrical section of the granule, at $T = 20\ d$, $T = 30\ d$, $T = 40\ d$, $T = 50\ d$, $T = 80\ d$. Wastewater influent composition: $S^{in}_{IC} = 180\ g\ m^{-3}$ (inorganic carbon), $S^{in}_{DOC} = 500\ g\ m^{-3}$ (organic carbon), $S^{in}_{NH_3} = 50\ g\ m^{-3}$ (ammonia), $S^{in}_{NO_3} = 0$ (nitrate), $S^{in}_{O_2} = 0$ (oxygen), $M^{in} = 100\ g\ m^{-3}$ (metal). Incident light intensity: $I_0 = 0.008\ kmol\ m^{-2}\ d^{-1}$. Duration of the cycle: $\tau = 6\ h$. Time of light exposure: $t_{light} = 50\%\ \tau$.

concentration can be observed across the granule: the free metal concentration goes from low values in a thin external layer to zero in the internal part.

Biofilm volume fractions and free binding sites volume fractions along the granule radius at different times are reported in Fig. 3. As shown in fig. 1, after 20 days the granule has achieved a radius of about 500 μm and the binding sites of each biofilm component are almost completely consumed. This is ascribed to the combination of different factors: high concentration of metal in the influent wastewater, which is rapidly adsorbed on the granule matrix, granules not completely developed and overall characterized by a small number of binding sites; low fraction of phototrophs throughout the granule. As shown in Fig. 2, when the phototrophs and EPS fractions start to be relevant ($T = 40\ d$), the adsorption process is favoured, microorganisms are less inhibited, and the granule radius increases. As a consequence, new free binding sites are formed and immediately occupied. Passing form $T = 40\ d$ to $T = 60\ d$ the granule radius undergoes a further significant increase (Fig. 1), and the residual metal concentration is completely adsorbed (see Fig. 4)

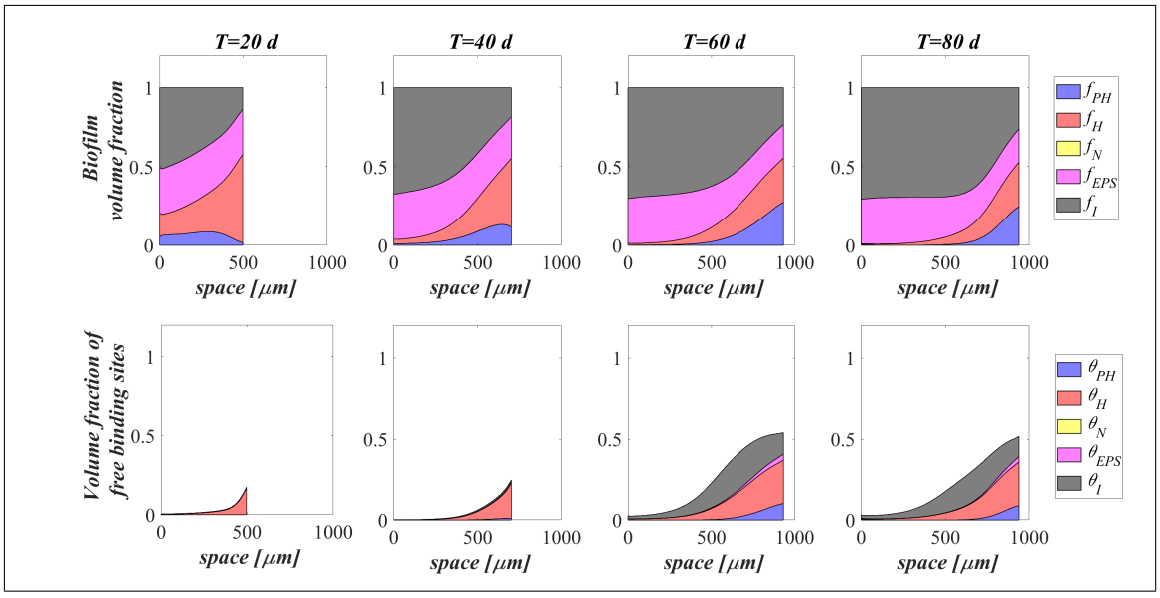


FIGURE 3. $SET1$ - Distribution of microbial species and free binding sites across the radius of the granule, at $T = 20\ d$, $T = 40\ d$, $T = 60\ d$, $T = 80\ d$. Wastewater influent composition: $S_{IC}^{in} = 180\ g\ m^{-3}$ (inorganic carbon), $S_{DOC}^{in} = 500\ g\ m^{-3}$ (organic carbon), $S_{NH_3}^{in} = 50\ g\ m^{-3}$ (ammonia), $S_{NO_3}^{in} = 0$ (nitrate), $S_{O_2}^{in} = 0$ (oxygen), $M^{in} = 100\ g\ m^{-3}$ (metal). Incident light intensity: $I_0 = 0.008\ kmol\ m^{-2}\ d^{-1}$. Duration of the cycle: $\tau = 6\ h$. Time of light exposure: $t_{light} = 50\%\ \tau$.

thanks to the high volume fractions of free binding sites. After 80 days the granule radius, microbial species distribution and volume fractions of free binding sites have achieved the steady-state configuration. Confirming what has been observed in Fig. 2, the granule is mainly composed by EPS, phototrophs, inert material, and heterotrophs. The residual binding sites still free indicates the algal-bacterial granules containing in the SBR are perfectly able to remove the metal present in the influent wastewater.

Fig. 4 reports the concentration of soluble substrates and metal within the reactor over time. The observation period includes the process start-up until the achievement of the steady-state representative of the working configuration of the reactor. It should be noted that such concentrations have a discontinuous trend, due to the SBR configuration. In the initial phase, the biofilm granules are small, and the consumption and production of soluble substrates are governed by planktonic biomass (see Fig. 6). Heterotrophic bacteria and phototrophs have higher growth rates than other microbial species. Thus, DOC (red) and NH_3 (cyan) consumption and IC (blue) production can be observed. When photogranules dimension increases, biological processes starts to be governed by sessile species. After 10 days, the oxygen (magenta) produced by phototrophs in presence of light is not sufficient for heterotrophs and nitrifiers, and no NO_3 (yellow) is present in the reactor. Thus, a temporary equilibrium in term of soluble substrates characterizes the system from 10 to 40 days. In this time frame, the metal (black) is slowly adsorbed on granules matrix and the metal inhibition effect on metabolic microbial activities reduces over time. As observed in Fig. 2, this favours phototrophs growth. Consequently, thanks to O_2 production (magenta), heterotrophic bacteria growth is promoted. Moreover, in this phase phototrophs are in turn responsible for more rapid metal adsorption, thanks

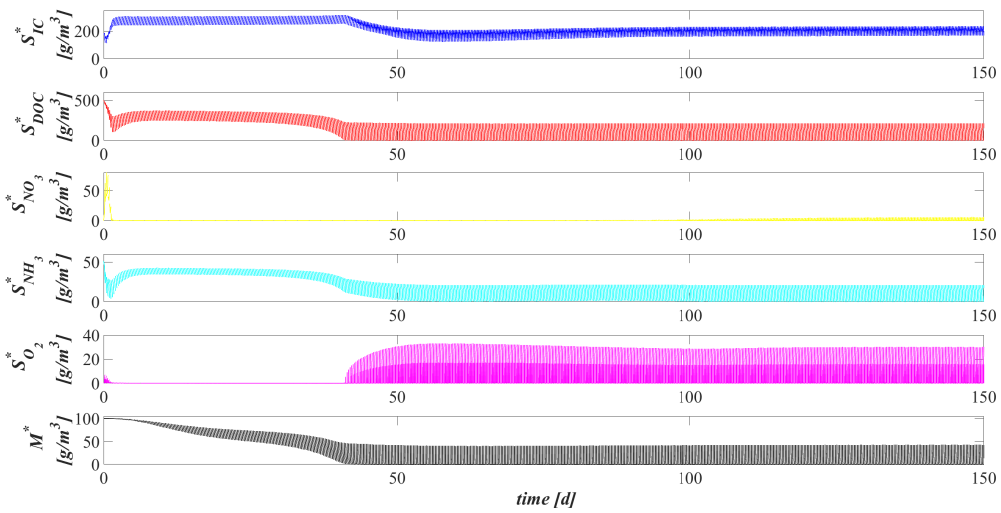


FIGURE 4. $SET1$ - Evolution of soluble substrates and metal concentrations within the reactor. Wastewater influent composition: $S^{in}_{IC} = 180\ g\ m^{-3}$ (inorganic carbon), $S^{in}_{DOC} = 500\ g\ m^{-3}$ (organic carbon), $S^{in}_{NH_3} = 50\ g\ m^{-3}$ (ammonia), $S^{in}_{NO_3} = 0$ (nitrate), $S^{in}_{O_2} = 0$ (oxygen), $M^{in} = 100\ g\ m^{-3}$ (metal). Incident light intensity: $I_0 = 0.008\ kmol\ m^{-2}\ d^{-1}$. Duration of the cycle: $\tau = 6\ h$. Time of light exposure: $t_{light} = 50\%\ \tau$.

to their elevate EPS productions and high adsorption capabilities. Metabolic activities of phototrophs and heterotrophs result in the complete NH_3 and DOC degradation, IC consumption, and M adsorption after $t = 60\ d$.

Once the photogranules have reached a steady-state dimension and microbial stratification, the trend of the substrates and metal concentrations are repeated identically in each cycle. Fig. 5 shows the evolution of the substrates and metal concentrations over time in the reactor in the period between 199 and 200 days. Note that each cycle identically repeats four times in a single day, and, for this reason, it is representative of the operating conditions of the system, while the substrates and metal concentrations at the end of each cycle are representative of the effluent composition. Solid lines represent the trends of IC (blue), DOC (red), NO_3 (yellow), NH_3 (cyan), O_2 (magenta), M (black) concentrations during the cycles. Each cycle is constituted by three hours of dark phase (gray parts of the graphs) and three hours of light phase (white parts of the graphs). While the circle and cross markers represent the concentrations of substrates and metal in the effluent and influent, respectively. At the end of each cycle (at 199.25, 199.50, 199.75, and 200 days) there is a discontinuity between the inlet and outlet concentration values, due to the procedure of emptying and refilling in the reactor. Due to the absence of light, in the first part of each cycle phototrophs and heterotrophs compete for O_2 (produced in the previous cycle), DOC and NH_3 producing IC. Contextually, a small amount of nitrifiers contributes to the conversion of O_2, IC and NH_3 into NO_3. When oxygen is completely consumed, anoxic heterotrophs grow consuming DOC and NO_3. When also the concentration of nitrate reaches zero, the trend of substrate concentrations does not show high variations until the end of the dark period. In light conditions, phototrophs carry out

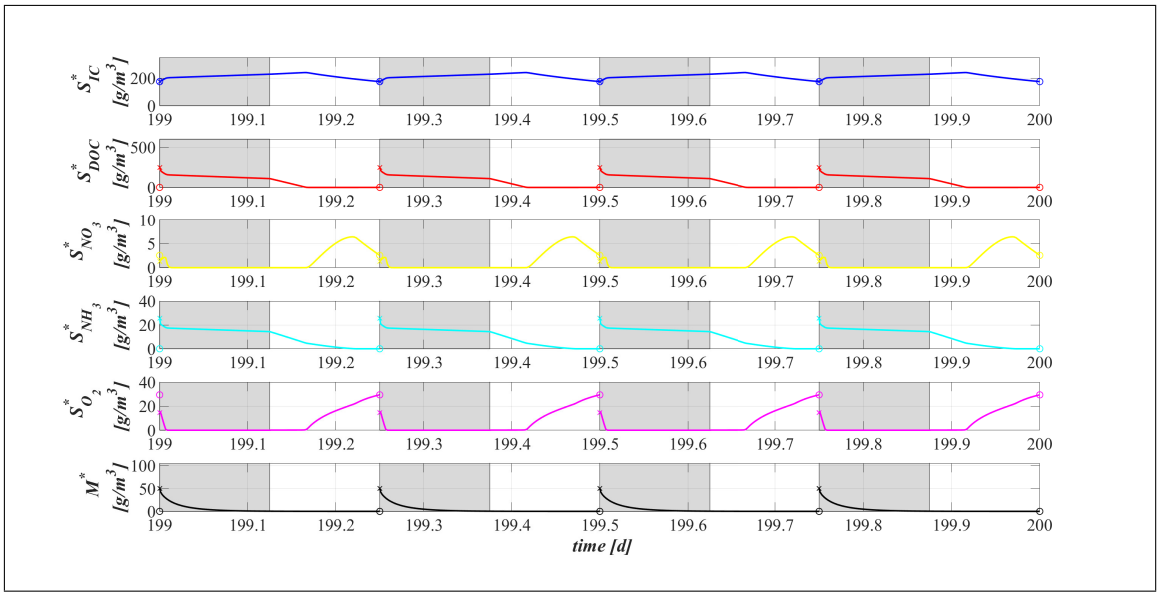


FIGURE 5. $SET1$ - Evolution of soluble substrates and metal concentrations within the reactor, from 199 d to 200 d (four consecutive six-hours treatment cycles). Wastewater influent composition: $S^{in}_{IC} = 180\ g\ m^{-3}$ (inorganic carbon), $S^{in}_{DOC} = 500\ g\ m^{-3}$ (organic carbon), $S^{in}_{NH_3} = 50\ g\ m^{-3}$ (ammonia), $S^{in}_{NO_3} = 0$ (nitrate), $S^{in}_{O_2} = 0$ (oxygen), $M^{in} = 100\ g\ m^{-3}$ (metal). Incident light intensity: $I_0 = 0.008\ kmol\ m^{-2}\ d^{-1}$. Duration of the cycle: $\tau = 6\ h$. Time of light exposure: $t_{light} = 50\%\ \tau$ (grey portions indicate the dark phases, white portions indicate the light phases).

photosynthesis, consuming NH_3 and IC, and producing large amount of O_2 necessary for heterotrophs and nitrifiers. Nevertheless, heterotrophic bacteria are more competitive in the use of O_2 in presence of DOC. As a result, the DOC concentration reduces and IC concentration increases. When the organic carbon ends, oxygen produced by phototrophs is used by nitrifying bacteria. For this reason, NH_3 and IC concentrations decreases, and NO_3 concentration increases. When also NH_3 is completely consumed, phototrophs grow on NO_3. At the end of the cycle, NH_3, DOC have been completely removed, and a very low concentrations of NO_3 (less than 5 $g\ m^{-3}$) and a concentration of about 30 $g\ m^{-3}$ of O_2 are observed. Indeed, the biomass of nitrifying bacteria within the granule and their growth rate are very low, therefore the production of NO_3 is limited. Regarding the metal adsorption, as already observed in Fig. 1 (top) at the steady-state the granule is mainly composed by phototrophs, EPS and inert material which are the major responsible for the adsorption process. Thus, during the day/night cycle the metal is completely adsorbed on granule matrix.

The concentration of planktonic and detached biomasses within the reactor over time is shown in Fig. 6. As for soluble substrates and metal (Fig. 4), the observation period includes the process start-up until the achievement of the steady-state representative of the working configuration of the reactor. Also in this case, such concentrations have a discontinuous trend, due to cyclic behaviour of the SBR. Several factors can affect the suspended biomasses evolution over time. Attachment phenomena contribute to decrease the concentrations of planktonic species, while detachment phenomena promote the growth of detached biomasses. Both types of biomasses grow on soluble substrates and decay.

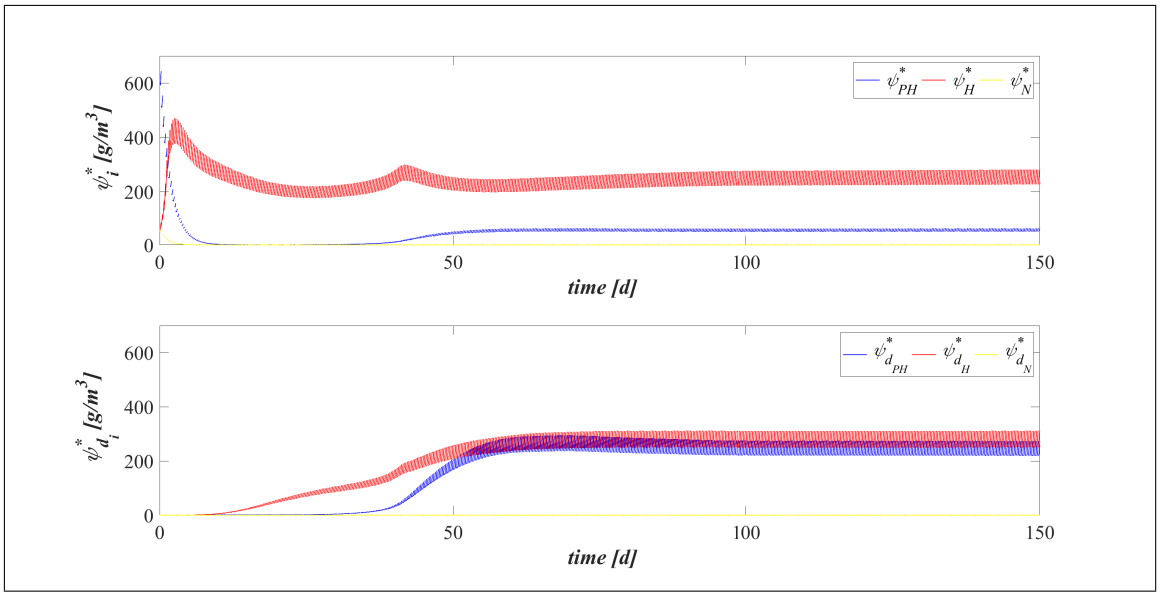


FIGURE 6. $SET1$ - Evolution of planktonic and detached biomasses concentrations within the reactor over time. Wastewater influent composition: $S^{in}_{IC} = 180\ g\ m^{-3}$ (inorganic carbon), $S^{in}_{DOC} = 500\ g\ m^{-3}$ (organic carbon), $S^{in}_{NH_3} = 50\ g\ m^{-3}$ (ammonia), $S^{in}_{NO_3} = 0$ (nitrate), $S^{in}_{O_2} = 0$ (oxygen), $M^{in} = 100\ g\ m^{-3}$ (metal). Incident light intensity: $I_0 = 0.008\ kmol\ m^{-2}\ d^{-1}$. Duration of the cycle: $\tau = 6\ h$. Time of light exposure: $t_{light} = 50\%\ \tau$.

Moreover, their concentration reduces during the emptying phase due to their non perfect settling properties. Lastly, detached biomasses reconvert into the planktonic cells after 48 h from the detachment. In the initial stage of the process, granules have still small dimension and there is an elevate availability of nutrients. As consequence, the substrates dynamics within the reactor are governed by planktonic biomass. Heterotrophic bacteria have higher growth rate than other microbial species, and their concentration rapidly increases. When the photogranules dimension increases, biological processes are governed by sessile species. Since then, the amount of substrates available for suspended biomass reduces and the concentration of heterotrophs in planktonic form decreases over time. Other species have low growth rates, and their concentrations decrease over time from the beginning of the process, due to the wash-out and attachment process. After 20 days, photogranules are already formed and the detachment process becomes relevant. This results in the increment of the concentration of heterotrophic detached biomass. Indeed, as shown in Fig. 2 the granule is initially composed by large amount of heterotrophs. After 40 days, sessile phototrophs grow within the granule and, consequently, the concentration of phototrophic detached biomass increases due to the detachment process. The conversion of heterotrophic and phototrophic detached biomasses into planktonic form causes a further increment of planktonic species. Subsequently, due to the shortage of DOC (Fig. 4) a slight reduction of planktonic species concentration within the bulk liquid can be observed again. Overall, after 60 days all suspended species within the reactor achieve a steady state value.

4.2. **SET2 - Effects of metal concentration on OPGs formation and adsorption processes.** Metals in wastewater may increase the sessile production of EPS, and, at the

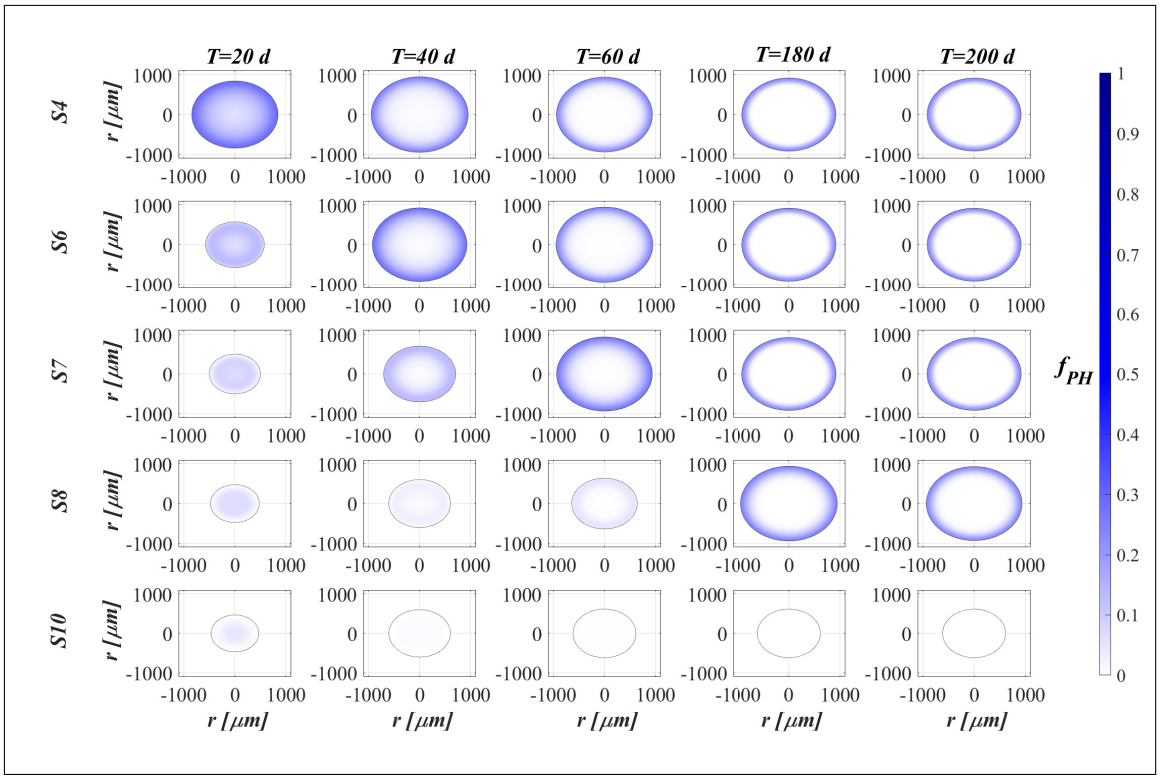


FIGURE 7. $SET2$ - Phototrophs distribution within the granule (diametrical section) at $T = 20\ d$, $T = 40\ d$, $T = 60\ d$, $T = 180\ d$, $T = 200\ d$ for different metal concentrations in the influent M^{in}. Wastewater influent composition: $S^{in}_{IC} = 180\ g\ m^{-3}$ (inorganic carbon), $S^{in}_{DOC} = 500\ g\ m^{-3}$ (organic carbon), $S^{in}_{NH_3} = 50\ g\ m^{-3}$ (ammonia), $S^{in}_{NO_3} = 0$ (nitrate), $S^{in}_{O_2} = 0$ (oxygen). $S4 : M^{in} = 40\ g\ m^{-3}$, $S6 : M^{in} = 80\ g\ m^{-3}$, $S7 : M^{in} = 100\ g\ m^{-3}$, $S8 : M^{in} = 120\ g\ m^{-3}$, $S10 : M^{in} = 160\ g\ m^{-3}$. Incident light intensity: $I_0 = 0.008\ kmol\ m^{-2}\ d^{-1}$. Duration of the cycle: $\tau = 6\ h$. Time of light exposure: $t_{light} = 50\%\ \tau$.

same time, may be the cause of stress conditions responsible for the death of microbial cells. More studies are necessary to identify a concentration range that allows microorganisms to grow and secrete EPS maximizing the removal efficiency of metals from wastewater. In this numerical study $SET2$, the efficiency of metal adsorption on the matrix of biofilm granules and the inhibiting effect on OPGs formation are investigated by considering different concentrations of metal. For this purpose, eleven simulations ($S2$ - $S12$) have been carried out by setting the concentration of metal in the influent M^{in} equal to 0, 20, 40, 60, 80, 100, 120, 140, 160, 180, 200 $g\ m^{-3}$. The concentration of soluble substrates in the influent wastewater S^{in}_j and initial concentration of planktonic biomasses within the reactor $\psi^*_{i,0}$ set for this numerical study are the same as in $SET1$. Numerical results are summarized in Figs. 7-12.

The concentration of metal in the influent affects the adsorption process as well as the microbial species stratification of OPGs. The distribution of the phototrophic sessile biomass at different times is reported in Fig. 7 for the following simulations: $S4$ ($M^{in} = 40\ g\ m^{-3}$), $S6$ ($M^{in} = 80\ g\ m^{-3}$), $S7$ ($M^{in} = 100\ g\ m^{-3}$), $S8$ ($M^{in} = 120\ g\ m^{-3}$), $S10$ ($M^{in} = 160\ g\ m^{-3}$). When the metal concentration present in the bioreactor is very

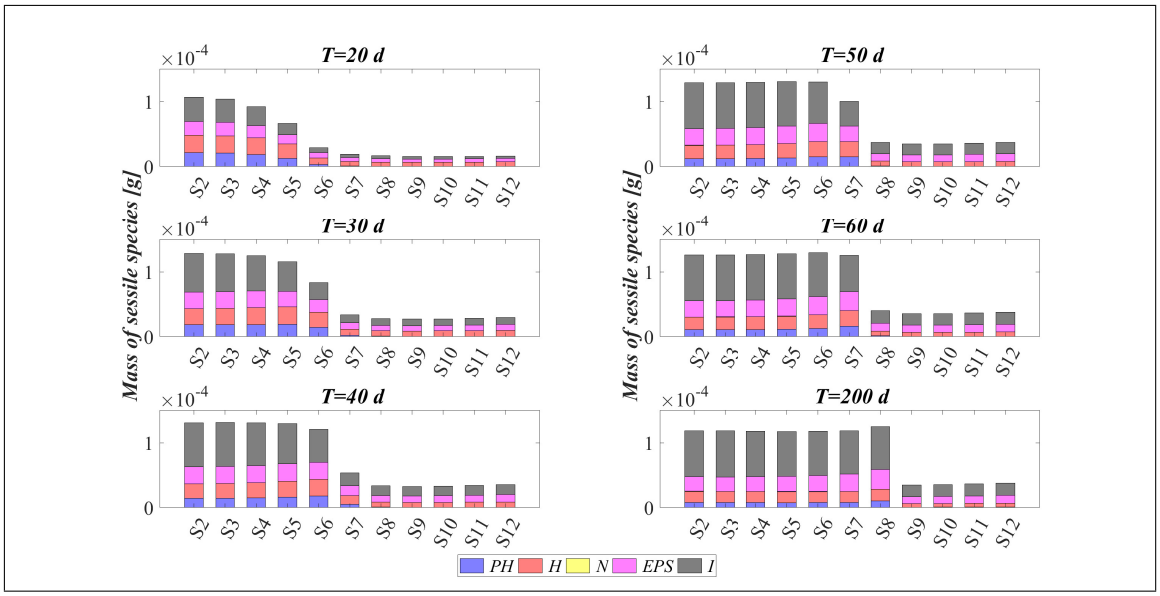


FIGURE 8. $SET2$ - Mass of microbial species within the granule at $T = 20\ d$, $T = 30\ d$, $T = 40\ d$, $T = 50\ d$, $T = 60\ d$, $T = 200\ d$ for different metal concentrations in the influent M^{in}. Wastewater influent composition: $S^{in}_{IC} = 180\ g\ m^{-3}$ (inorganic carbon), $S^{in}_{DOC} = 500\ g\ m^{-3}$ (organic carbon), $S^{in}_{NH_3} = 50\ g\ m^{-3}$ (ammonia), $S^{in}_{NO_3} = 0$ (nitrate), $S^{in}_{O_2} = 0$ (oxygen). $S2 : M^{in} = 0$, $S3 : M^{in} = 20\ g\ m^{-3}$, $S4 : M^{in} = 40\ g\ m^{-3}$, $S5 : M^{in} = 60\ g\ m^{-3}$, $S6 : M^{in} = 80\ g\ m^{-3}$, $S7 : M^{in} = 100\ g\ m^{-3}$, $S8 : M^{in} = 120\ g\ m^{-3}$, $S9 : M^{in} = 140\ g\ m^{-3}$, $S10 : M^{in} = 160\ g\ m^{-3}$, $S11 : M^{in} = 180\ g\ m^{-3}$, $S12 : M^{in} = 200\ g\ m^{-3}$. Incident light intensity: $I_0 = 0.008\ kmol\ m^{-2}\ d^{-1}$. Duration of the cycle: $\tau = 6\ h$. Time of light exposure: $t_{light} = 50\%\ \tau$.

low ($S4$), phototrophs are less inhibited and grow faster within the granule. Conversely, a higher concentration of free metal results in a higher inhibition effect and leads to a slower growth of phototrophs. It means that for wastewater richer in metal the growth of the phototrophic species and the adsorption process occur in a longer time. Thus, the maximum fraction of phototrophs is observed later going from $S4$ to $S8$. However, after long times the phototrophs distribution is no longer affected by M^{in} and all simulations achieve the same steady-state configuration after 200 days, except for $M^{in} = 160\ g\ m^{-3}$. Indeed, in this case ($S10$) the metal concentration is too high, and the biomasses growth and the granule formation are strongly inhibited by the presence of free metal. As a result, the photogranule does not completely develop and the absence of phototrophs is observed throughout the granule at 200 days.

This is visible also in Fig. 8, where the mass of sessile microbial species within the granule is shown at different times. Relevant differences concern the initial phase of the process when the total sessile mass is higher for low metal concentrations. However, after long times (when the adsorption process is completed) the sessile mass of the individual microbial species within the granule is no longer affected by the presence of metal for M^{in} lower than $140\ g\ m^{-3}$.

The evolution of the granule radius $R(t)$ over time is shown in Fig. 9. M^{in} affects the granule evolution in the initial stage of the process. For low concentrations of metal, the

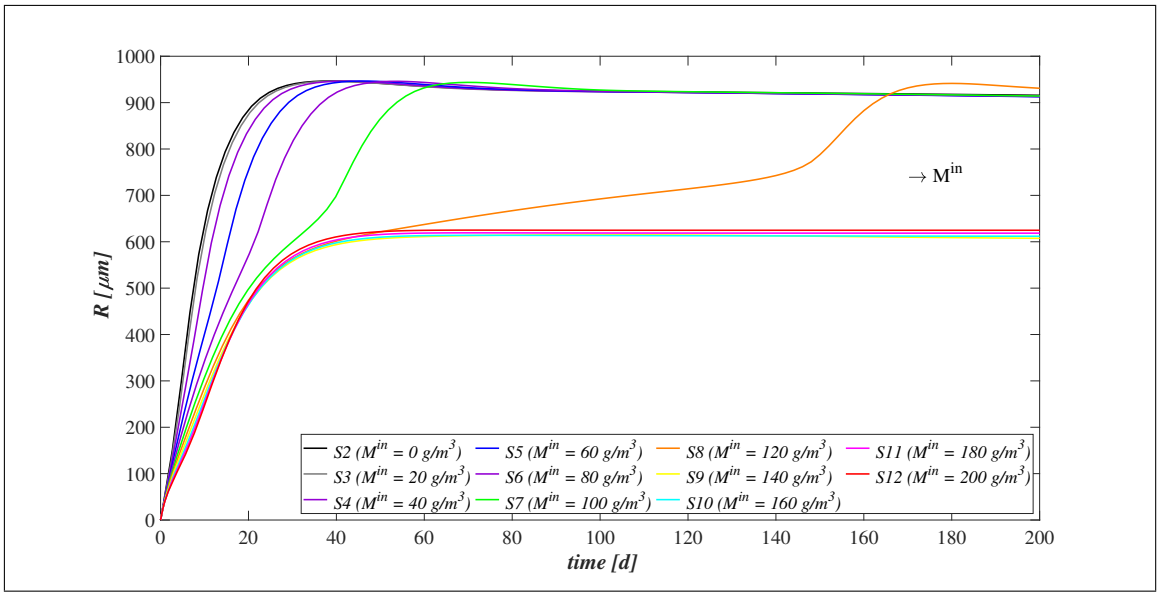


FIGURE 9. $SET2$ - Biofilm radius evolution over time for different metal concentrations in the influent M^{in}. Wastewater influent composition: $S^{in}_{IC} = 180\ g\ m^{-3}$ (inorganic carbon), $S^{in}_{DOC} = 500\ g\ m^{-3}$ (organic carbon), $S^{in}_{NH_3} = 50\ g\ m^{-3}$ (ammonia), $S^{in}_{NO_3} = 0$ (nitrate), $S^{in}_{O_2} = 0$ (oxygen). $S2 : M^{in} = 0$, $S3 : M^{in} = 20\ g\ m^{-3}$, $S4 : M^{in} = 40\ g\ m^{-3}$, $S5 : M^{in} = 60\ g\ m^{-3}$, $S6 : M^{in} = 80\ g\ m^{-3}$, $S7 : M^{in} = 100\ g\ m^{-3}$, $S8 : M^{in} = 120\ g\ m^{-3}$, $S9 : M^{in} = 140\ g\ m^{-3}$, $S10 : M^{in} = 160\ g\ m^{-3}$, $S11 : M^{in} = 180\ g\ m^{-3}$, $S12 : M^{in} = 200\ g\ m^{-3}$. Incident light intensity: $I_0 = 0.008\ kmol\ m^{-2}\ d^{-1}$. Duration of the cycle: $\tau = 6\ h$. Time of light exposure: $t_{light} = 50\%\ \tau$.

granule radius increases earlier, small inhibiting effects are observed during the granulation process, and the adsorption process is faster completed. When M^{in} is higher or equal to $100\ g\ m^{-3}$, the granule partially grows, and a further radius increment associated to phototrophs growth can be observed later. Note that passing from $S6$ to $S8$ the phototrophs growth and the subsequent further increment of the granule radius are increasingly slowed down by the presence of free metal, as observed in Fig. 7. Instead, when M^{in} is equal to 140, 160, 180 and 200 $g\ m^{-3}$ the phototrophic biomass growth is totally inhibited. Hence, the absence of phototrophs observed in Fig. 7 and Fig. 8 is confirmed by the incomplete development of the granule.

The metal and substrates concentrations in the effluent after each SBR cycle are displayed in Fig. 10 and 11. Each point represents the concentrations of metal and substrates in the effluent at the end of each cycle. Fig. 10 shows that for low metal concentration in the influent wastewater, the adsorption process is rapid and almost linear. When M^{in} is equal to 100 and 120 $g\ m^{-3}$, the removal process slows down at $T = 20\ d$. The phototrophic biomass is characterized by lower growth rate than heterotrophs, and the inhibiting effect related to the presence of free metal further limits their growth process. Later, after 30 days, a considerable growth of phototrophs allows to successfully complete the adsorption process. Specifically, higher is the metal concentration in the influent and slower is the adsorption process. This is related to two aspects: the amount of free metal to adsorb is larger, and the phototrophs growth is slower due to the stronger metal inhibition effect.

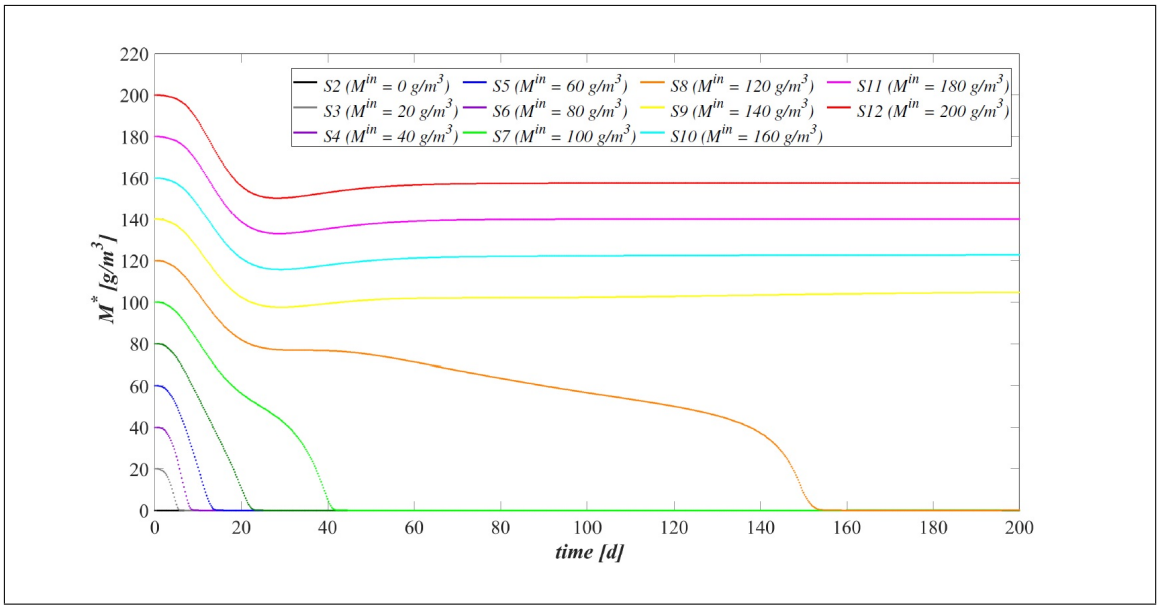


FIGURE 10. $SET2$ - Metal concentration evolution within the reactor for different metal concentrations in the influent M^{in}. Wastewater influent composition: $S^{in}_{IC} = 180\ g\ m^{-3}$ (inorganic carbon), $S^{in}_{DOC} = 500\ g\ m^{-3}$ (organic carbon), $S^{in}_{NH_3} = 50\ g\ m^{-3}$ (ammonia), $S^{in}_{NO_3} = 0$ (nitrate), $S^{in}_{O_2} = 0$ (oxygen). $S2 : M^{in} = 0$, $S3 : M^{in} = 20\ g\ m^{-3}$, $S4 : M^{in} = 40\ g\ m^{-3}$, $S5 : M^{in} = 60\ g\ m^{-3}$, $S6 : M^{in} = 80\ g\ m^{-3}$, $S7 : M^{in} = 100\ g\ m^{-3}$, $S8 : M^{in} = 120\ g\ m^{-3}$, $S9 : M^{in} = 140\ g\ m^{-3}$, $S10 : M^{in} = 160\ g\ m^{-3}$, $S11 : M^{in} = 180\ g\ m^{-3}$, $S12 : M^{in} = 200\ g\ m^{-3}$. Incident light intensity: $I_0 = 0.008\ kmol\ m^{-2}\ d^{-1}$. Duration of the cycle: $\tau = 6\ h$. Time of light exposure: $t_{light} = 50\%\ \tau$.

As shown in Fig. 8, for M^{in} higher or equal to 140 $g\ m^{-3}$ the granule is not completely developed, and a small amount of EPS and a not visible fraction of phototrophs are present in the granule. Consequently, the adsorption process is not yet completed after 200 days.

The effluent concentration of soluble substrates is reported in Fig. 11. The initial phase of the process, in which DOC and NH_3 are consumed and IC is produced, is faster when the metal concentration in the influent is lower. Indeed, the inhibiting effect delays the granulation process and, as consequence, the substrates consumption/production. The subsequent phase is governed by phototrophs, which promote the metabolic activities of the heterotrophic bacteria producing O_2. When M^{in} is higher, phototrophs growth is slower, and oxygen is less rapidly produced. As a result, time necessary to reach the complete degradation of DOC and NH_3 and the maximum IC reduction increases. Specifically, the same effluent composition both in terms of metal (Fig. 10) and substrates (Fig. 11) is achieved at the steady-state for M^{in} lower than 140 $g\ m^{-3}$. While, in the other cases the degradation of nutrients and metal adsorption only partially occur.

The steady-state configuration of the residual free binding sites within the biofilm granule is reported in Fig. 12. Obviously, when no metal is present in the influent wastewater ($S2$), no adsorption site is occupied during the granulation process and the sum of all volume fractions returns 1 at each location and time. The numerical results show that, for values of M^{in} between 20 and 120 $g\ m^{-3}$, the adsorption process requires a growing number of binding sites. Consequently, a decreasing residual amount of adsorption sites

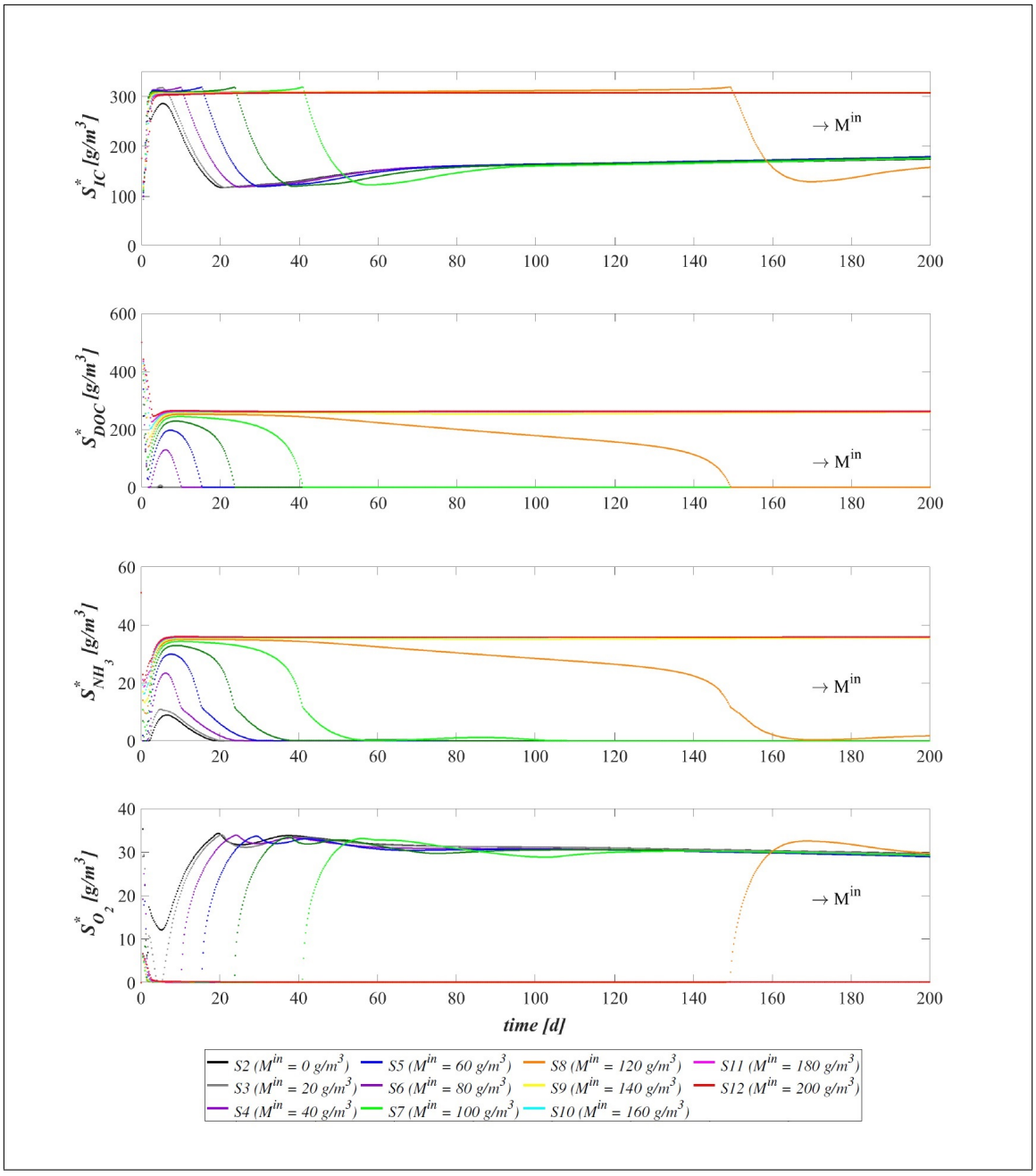


FIGURE 11. $SET2$ - Evolution of soluble substrates concentration within the reactor for different metal concentrations in the influent M^{in}. Wastewater influent composition: $S^{in}_{IC} = 180\ g\ m^{-3}$ (inorganic carbon), $S^{in}_{DOC} = 500\ g\ m^{-3}$ (organic carbon), $S^{in}_{NH_3} = 50\ g\ m^{-3}$ (ammonia), $S^{in}_{NO_3} = 0$ (nitrate), $S^{in}_{O_2} = 0\ g\ m^{-3}$ (oxygen). $S2 : M^{in} = 0$, $S3 : M^{in} = 20\ g\ m^{-3}$, $S4 : M^{in} = 40\ g\ m^{-3}$, $S5 : M^{in} = 60\ g\ m^{-3}$, $S6 : M^{in} = 80\ g\ m^{-3}$, $S7 : M^{in} = 100\ g\ m^{-3}$, $S8 : M^{in} = 120\ g\ m^{-3}$, $S9 : M^{in} = 140\ g\ m^{-3}$, $S10 : M^{in} = 160\ g\ m^{-3}$, $S11 : M^{in} = 180\ g\ m^{-3}$, $S12 : M^{in} = 200\ g\ m^{-3}$. Incident light intensity: $I_0 = 0.008\ kmol\ m^{-2}\ d^{-1}$. Duration of the cycle: $\tau = 6\ h$. Time of light exposure: $t_{light} = 50\%\ \tau$.

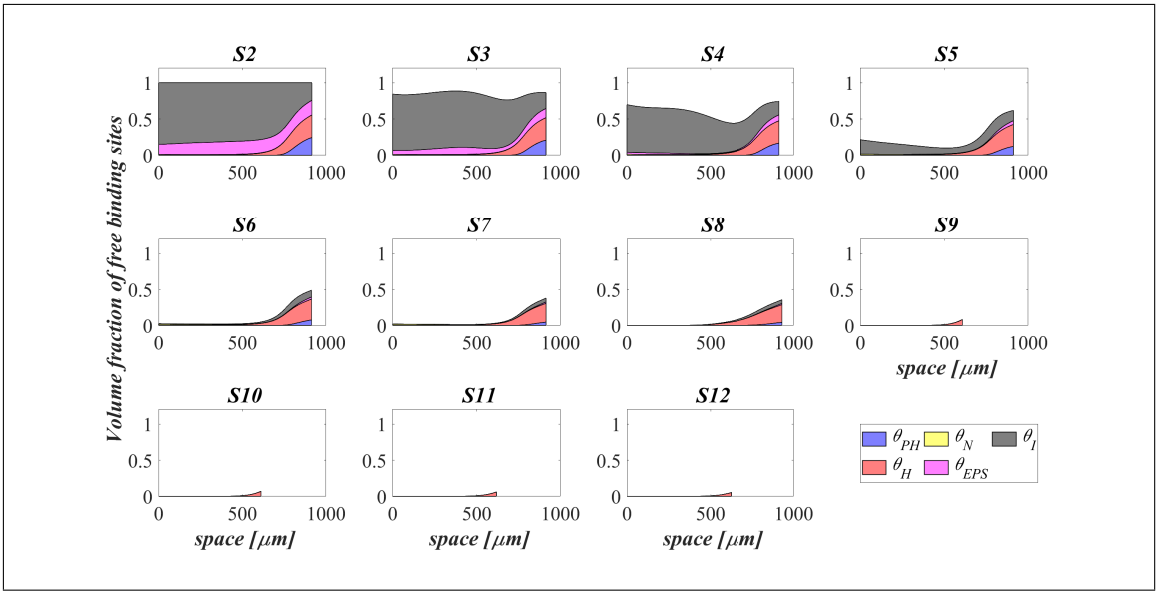


FIGURE 12. $SET2$ - Distribution of the residual free binding site across the radius of the granule for different metal concentrations in the influent M^{in} at $T = 200\ d$. Wastewater influent composition: $S^{in}_{IC} = 180\ g\ m^{-3}$ (inorganic carbon), $S^{in}_{DOC} = 500\ g\ m^{-3}$ (organic carbon), $S^{in}_{NH_3} = 50\ g\ m^{-3}$ (ammonia), $S^{in}_{NO_3} = 0$ (nitrate), $S^{in}_{O_2} = 0$ (oxygen). $S2 : M^{in} = 0$, $S3 : M^{in} = 20\ g\ m^{-3}$, $S4 : M^{in} = 40\ g\ m^{-3}$, $S5 : M^{in} = 60\ g\ m^{-3}$, $S6 : M^{in} = 80\ g\ m^{-3}$, $S7 : M^{in} = 100\ g\ m^{-3}$, $S8 : M^{in} = 120\ g\ m^{-3}$, $S9 : M^{in} = 140\ g\ m^{-3}$, $S10 : M^{in} = 160\ g\ m^{-3}$, $S11 : M^{in} = 180\ g\ m^{-3}$, $S12 : M^{in} = 200\ g\ m^{-3}$. Incident light intensity: $I_0 = 0.008\ kmol\ m^{-2}\ d^{-1}$. Duration of the cycle: $\tau = 6\ h$. Time of light exposure: $t_{light} = 50\%\ \tau$.

can be observed, although the granule achieves the same steady-state dimension. Lastly, in the cases in which the metal concentration is too high, the adsorption process is not completed (from $S9$ to $S12$), the granule does not completely develop due to the stronger inhibiting effect, and the binding sites are almost occupied.

4.3. **SET3 - Effects of metal adsorption capabilities on OPGs formation and adsorption processes.** Experimental works show that heat or acid pretreatments enhance the metal adsorption potential of algal-bacterial biomass [38]. Metal affinity to the biomass could be manipulated by pretreating the biomass with alkalies, acids, detergents, and heat, which may increase the amount of adsorbed metal and reduce the time necessary for the adsorption process [52]. Indeed, a physical/chemical pretreatment affects the permeability and surface charge of the biomass and makes the adsorption sites more accessible for metal biosorption [4]. In this context, a numerical study ($SET3$) is performed to investigate the pretreatment effect on the evolution of biofilm granules and metal removal. Five simulations ($S13$-$S17$) have been carried out using different values of binding sites densities ρ_θ.

The five values of ρ_θ used are: 10, 20, 30, 40, 50 $N^{\circ}_{sites}\ m^{-3}$. The concentration of soluble substrates in the influent wastewater S^{in}_j and initial concentration of planktonic biomasses within the reactor $\psi^{*}_{i,0}$ set for this numerical study are the same as in $SET1$. Numerical results are summarized in Figs. 13-18.

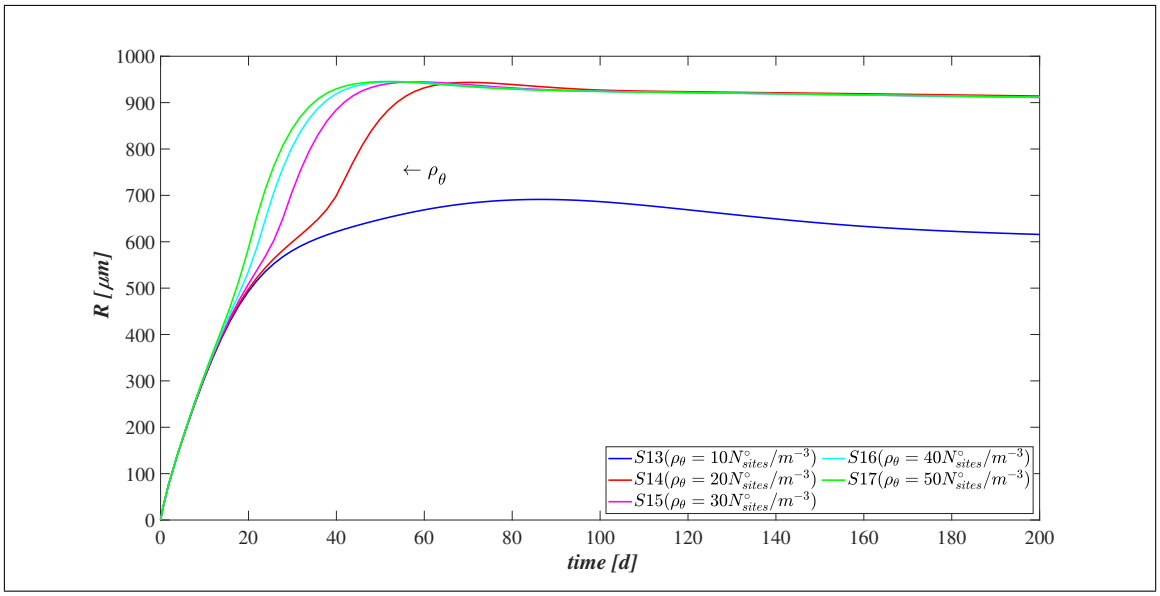


FIGURE 13. $SET3$ - Biofilm radius evolution over time for different densities of binding sites ρ_θ. Wastewater influent composition: $S^{in}_{IC} = 180\ g\ m^{-3}$ (inorganic carbon), $S^{in}_{DOC} = 500\ g\ m^{-3}$ (organic carbon), $S^{in}_{NH_3} = 50\ g\ m^{-3}$ (ammonia), $S^{in}_{NO_3} = 0$ (nitrate), $S^{in}_{O_2} = 0$ (oxygen). $S13 : \rho_\theta = 10\ N^\circ_{sites}\ m^{-3}$, $S14 : \rho_\theta = 20\ N^\circ_{sites}\ m^{-3}$, $S15 : \rho_\theta = 30\ N^\circ_{sites}\ m^{-3}$, $S16 : \rho_\theta = 40\ N^\circ_{sites}\ m^{-3}$, $S17 : \rho_\theta = 50\ N^\circ_{sites}\ m^{-3}$. Incident light intensity: $I_0 = 0.008\ kmol\ m^{-2}\ d^{-1}$. Duration of the cycle: $\tau = 6\ h$. Time of light exposure: $t_{light} = 50\%\ \tau$.

The time evolution of the granule radius $R(t)$ is shown in Fig. 13. It is clear that different densities of binding sites ρ_θ affects the granule evolution in the second stage of the process, since the further radius increment around 20-50 days is associated to the phototrophs growth and phototrophs and EPS have better adsorption capabilities. Indeed, when ρ_θ increases, the granulation process occurs rapidly and the granule reaches the steady-state size quickly. However, such steady-state size is not dependent on the binding sites density. Indeed, the profiles of $R(t)$ get closer over time and reach the same steady-state value, except for $\rho_\theta = 10\ N^\circ_{sites}\ m^{-3}$. It leads to conclude that with very low densities of binding sites the granulation and adsorption process do not completely evolve.

Fig. 14 reports the sessile mass of the different microbial species within the granule. Again, relevant differences concern phototrophs growth. The phototrophs mass increases faster when the algal-bacterial consortium have higher binding sites densities. Metal removal and phototrophs growth positively influence each other. A faster metal adsorption enhances the phototrophic growth rate, and phototrophs contribute to accelerate the metal removal process thanks to their high adsorption properties.

This is visible also in Fig. 15, where the phototrophic sessile biomass within the granule is shown at different times. Again, relevant differences concern the time frame which goes from 20 to 50 days. By increasing ρ_θ, phototrophic sessile biomass grows faster and the steady-state microbial distribution is reached earlier. However, the steady-state distribution is the same for all values of densities, except for the simulation $S13$, in which no phototrophic biomass is detected throughout the granule.

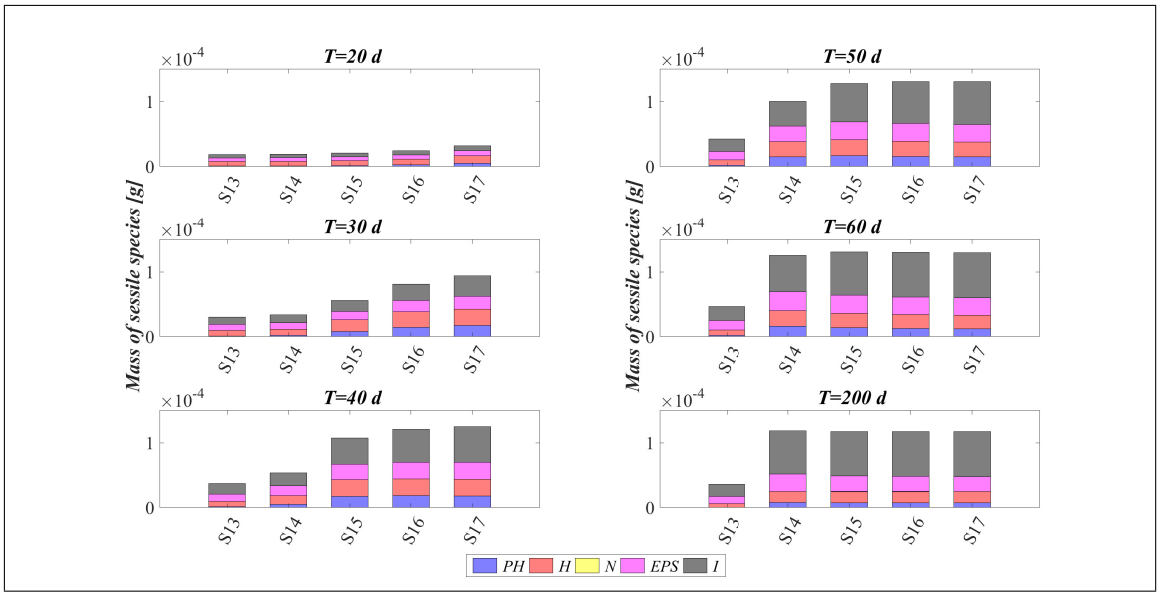


FIGURE 14. $SET3$ - Mass of microbial species within the granule at $T = 20\ d$, $T = 30\ d$, $T = 40\ d$, $T = 50\ d$, $T = 60\ d$, $T = 200\ d$ for different densities of binding sites ρ_θ. Wastewater influent composition: $S^{in}_{IC} = 180\ g\ m^{-3}$ (inorganic carbon), $S^{in}_{DOC} = 500\ g\ m^{-3}$ (organic carbon), $S^{in}_{NH_3} = 50\ g\ m^{-3}$ (ammonia), $S^{in}_{NO_3} = 0$ (nitrate), $S^{in}_{O_2} = 0$ (oxygen). $S13 : \rho_\theta = 10\ N^{\circ}_{sites}\ m^{-3}$, $S14 : \rho_\theta = 20\ N^{\circ}_{sites}\ m^{-3}$, $S15 : \rho_\theta = 30\ N^{\circ}_{sites}\ m^{-3}$, $S16 : \rho_\theta = 40\ N^{\circ}_{sites}\ m^{-3}$, $S17 : \rho_\theta = 50\ N^{\circ}_{sites}\ m^{-3}$. Incident light intensity: $I_0 = 0.008\ kmol\ m^{-2}\ d^{-1}$. Duration of the cycle: $\tau = 6\ h$. Time of light exposure: $t_{light} = 50\%\ \tau$.

Fig. 16 presents the steady-state configuration of the residual free binding sites within the biofilm granule. Obviously, for ρ_θ equal to $10\ N^{\circ}_{sites}\ m^{-3}$ the adsorption process is not completed ($S13$), the granule does not completely develop due to the stronger inhibiting effect, and the binding sites are almost occupied. On the contrary, for higher values of binding sites density an increasing residual fraction of adsorption sites can be observed ($S14 - S17$).

Fig. 17 and 18 show the trend of soluble substrates and metal concentrations in the SBR effluent, respectively. Each point represents the concentrations of substrates and metal in the effluent at the end of each cycle. As mentioned before, in the initial stage of the process the consumption and production of soluble substrates mainly depend on the metabolic activity of heterotrophic biomass. Consequently, the trends of soluble substrates are not affected by the variation of ρ_θ, since the role of heterotrophic bacteria in the adsorption process is marginal. For later times, phototrophic biomass starts to grow, and the trend of substrates (Fig. 17) and metal (Fig. 18) becomes more sensitive to ρ_θ. For high values of ρ_θ, the concentrations of soluble substrates and metal achieve the steady-state values earlier and the time required to completely adsorb the residual metal decreases. For $\rho_\theta = 10\ N^{\circ}_{sites}\ m^{-3}$, the metal adsorption process does not complete, because of the absence of phototrophs and the small amount of EPS observed throughout the granule.

From the numerical results, it is clear that the density of binding sites ρ_θ influences the adsorption process rate of the free metal, and, therefore, the time necessary for the metal removal. Anyway, it can be concluded that the steady-state configuration in terms

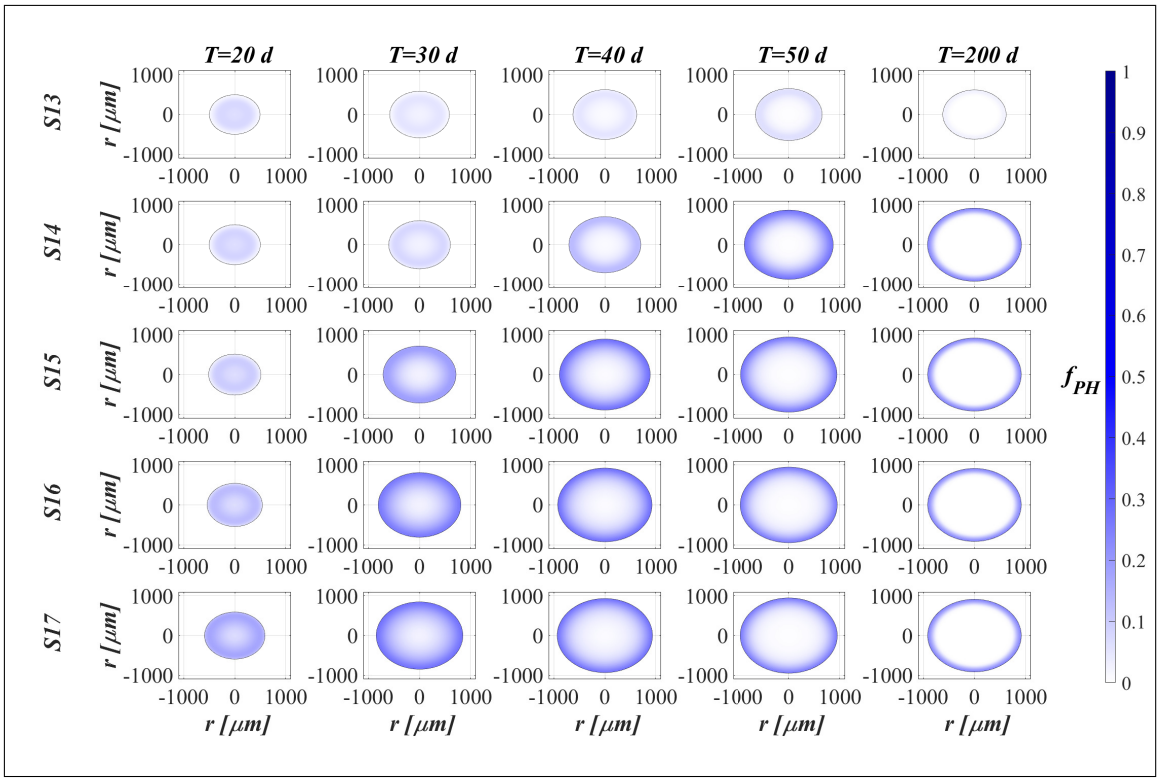


FIGURE 15. $SET3$ - Phototrophs distribution within the granule (diametrical section) at $T = 20\ d$, $T = 30\ d$, $T = 40\ d$, $T = 50\ d$, $T = 200\ d$ for different densities of binding sites ρ_θ. Wastewater influent composition: $S^{in}_{IC} = 180\ g\ m^{-3}$ (inorganic carbon), $S^{in}_{DOC} = 500\ g\ m^{-3}$ (organic carbon), $S^{in}_{NH_3} = 50\ g\ m^{-3}$ (ammonia), $S^{in}_{NO_3} = 0$ (nitrate), $S^{in}_{O_2} = 0$ (oxygen). $S13 : \rho_\theta = 10\ N^{\circ}_{sites}\ m^{-3}$, $S14 : \rho_\theta = 20\ N^{\circ}_{sites}\ m^{-3}$, $S15 : \rho_\theta = 30\ N^{\circ}_{sites}\ m^{-3}$, $S16 : \rho_\theta = 40\ N^{\circ}_{sites}\ m^{-3}$, $S17 : \rho_\theta = 50\ N^{\circ}_{sites}\ m^{-3}$. Incident light intensity: $I_0 = 0.008\ kmol\ m^{-2}\ d^{-1}$. Duration of the cycle: $\tau = 6\ h$. Time of light exposure: $t_{light} = 50\%\ \tau$.

of biofilm dimension, microbial species stratification, and metal removal efficiency of the process are not affected by ρ_θ above a critical value.

5. Discussion and conclusions

Biosorption is proving to be a promising alternative to conventional methods for the removal of metals from municipal and industrial effluents, as microorganisms and their derived products have high biosorption capabilities of inorganic compounds. Indeed, conventional physico/chemical methods for metals removal are expensive and inefficient for very low metals concentrations [4, 1, 6, 3]. Biosorption offers several advantages including cost effectiveness, high efficiency, minimization of chemical compounds utilization, and regeneration of biosorbents [4]. Nevertheless, there are practical limitations as living biomass is very sensitive to high metal concentrations [14]. An understanding of metal toxicity effects in biofilms is crucial to the successfully design bioreactors for the contextual removal of organic contaminants and metals. The mathematical model proposed in this work allows to simulate the formation and evolution of oxygenic photogranules within a granular-based sequencing batch reactor and describing the adsorption process of metals

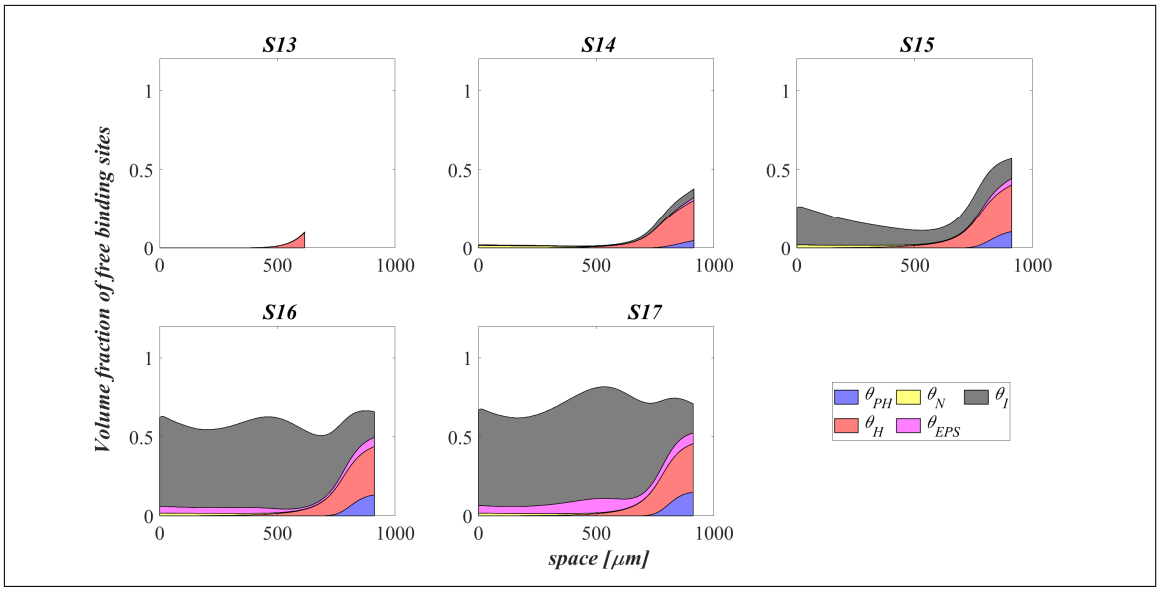


FIGURE 16. $SET3$ - Distribution of the residual free binding site across the radius of the granule for different densities of binding sites ρ_θ at $T = 200\ d$. Wastewater influent composition: $S^{in}_{IC} = 180\ g\ m^{-3}$ (inorganic carbon), $S^{in}_{DOC} = 500\ g\ m^{-3}$ (organic carbon), $S^{in}_{NH_3} = 50\ g\ m^{-3}$ (ammonia), $S^{in}_{NO_3} = 0$ (nitrate), $S^{in}_{O_2} = 0$ (oxygen). $S13 : \rho_\theta = 10\ N^{\circ}_{sites}\ m^{-3}$, $S14 : \rho_\theta = 20\ N^{\circ}_{sites}\ m^{-3}$, $S15 : \rho_\theta = 30\ N^{\circ}_{sites}\ m^{-3}$, $S16 : \rho_\theta = 40\ N^{\circ}_{sites}\ m^{-3}$, $S17 : \rho_\theta = 50\ N^{\circ}_{sites}\ m^{-3}$. Incident light intensity: $I_0 = 0.008\ kmol\ m^{-2}\ d^{-1}$. Duration of the cycle: $\tau = 6\ h$. Time of light exposure: $t_{light} = 50\%\ \tau$.

on the matrix of biofilm granules. The most interesting observations resulting from the numerical studies are summarized below:

- The adsorption process on oxygenic photogranules matrix shows high removal efficiency. These numerical result is in accordance with experimental works in which more than 99% of metal present in aqueous solutions is absorbed using algal-bacterial granules, thanks to their excellent adsorption capacities [2, 18, 19].
- The results outline the key role of phototrophs and EPS in the metal removal process, as phototrophs are good biosorbents and metals stimulate the production of EPS in greater amount and with higher adsorption capabilities. These results reflect what has been observed in Yang et al. [18], where a comparison between conventional bacterial granules and algal-bacterial photogranules is performed, demonstrating that algal-bacterial granular biofilms show advantages in both biosorption capacity and granular stability.
- Furthermore, the model confirms that the performances of the adsorption process can be significantly affected by the metals concentration present in the wastewater. The highest removal efficiencies are achieved for low concentrations of metal in the influent [4]. Indeed, higher is the metal concentration in the influent and stronger will be the inhibiting effect on the microbial growth. Although EPS content significantly increases in presence of metals [2], numerical results show that it is not sufficient in case of very high metal concentration. Moreover, as shown by Yang et al. [2], biomass growth is not or is little inhibited by certain concentrations of

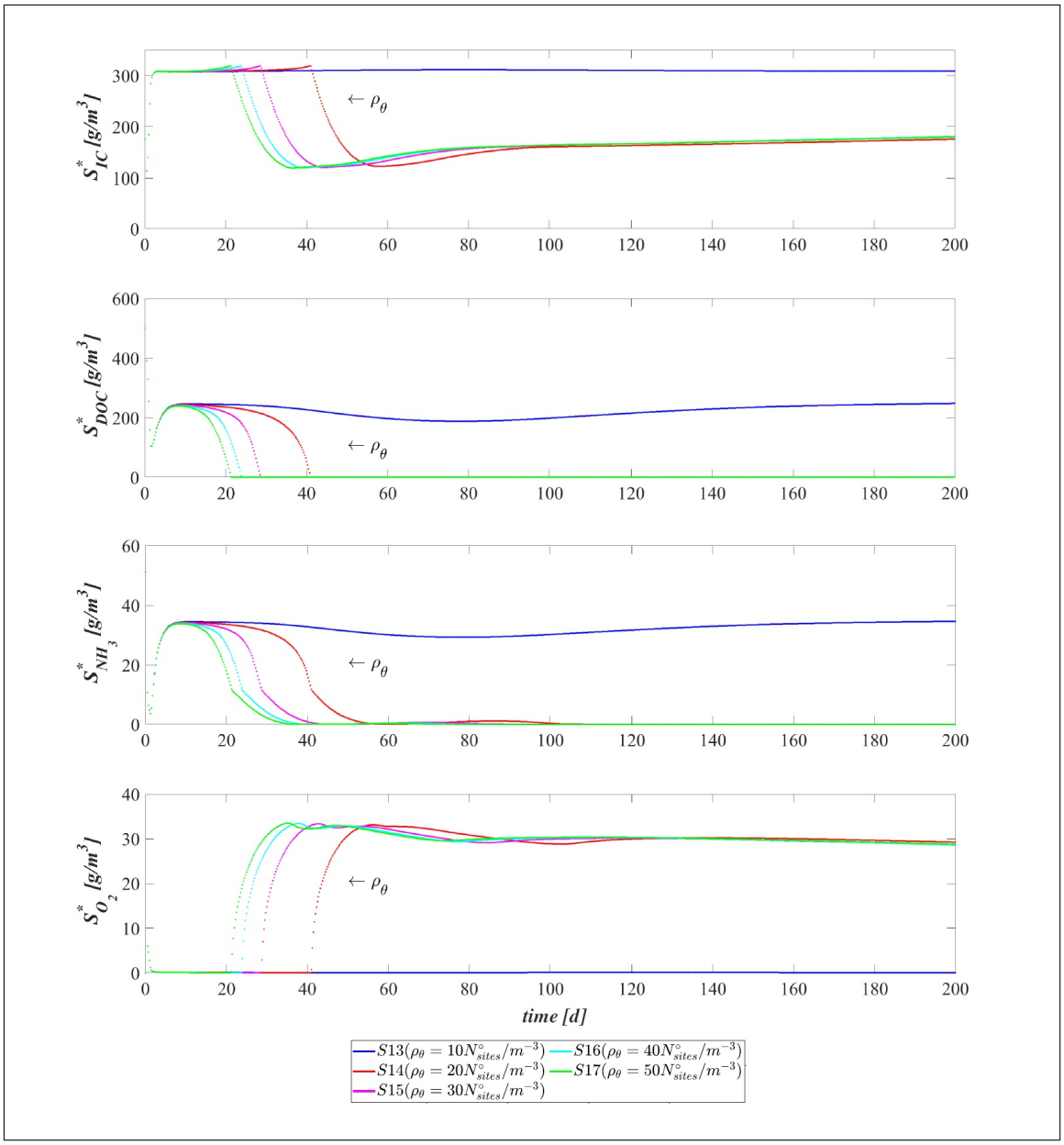


FIGURE 17. $SET3$ - Soluble substrates concentration evolution within the reactor for different densities of binding sites ρ_θ. Wastewater influent composition: $S^{in}_{IC} = 180\ g\ m^{-3}$ (inorganic carbon), $S^{in}_{DOC} = 500\ g\ m^{-3}$ (organic carbon), $S^{in}_{NH_3} = 50\ g\ m^{-3}$ (ammonia), $S^{in}_{NO_3} = 0$ (nitrate), $S^{in}_{O_2} = 0$ (oxygen). $S13 : \rho_\theta = 10\ N^\circ_{sites}\ m^{-3}$, $S14 : \rho_\theta = 20\ N^\circ_{sites}\ m^{-3}$, $S15 : \rho_\theta = 30\ N^\circ_{sites}\ m^{-3}$, $S16 : \rho_\theta = 40\ N^\circ_{sites}\ m^{-3}$, $S17 : \rho_\theta = 50\ N^\circ_{sites}\ m^{-3}$. Incident light intensity: $I_0 = 0.008\ kmol\ m^{-2}\ d^{-1}$. Duration of the cycle: $\tau = 6\ h$. Time of light exposure: $t_{light} = 50\%\ \tau$.

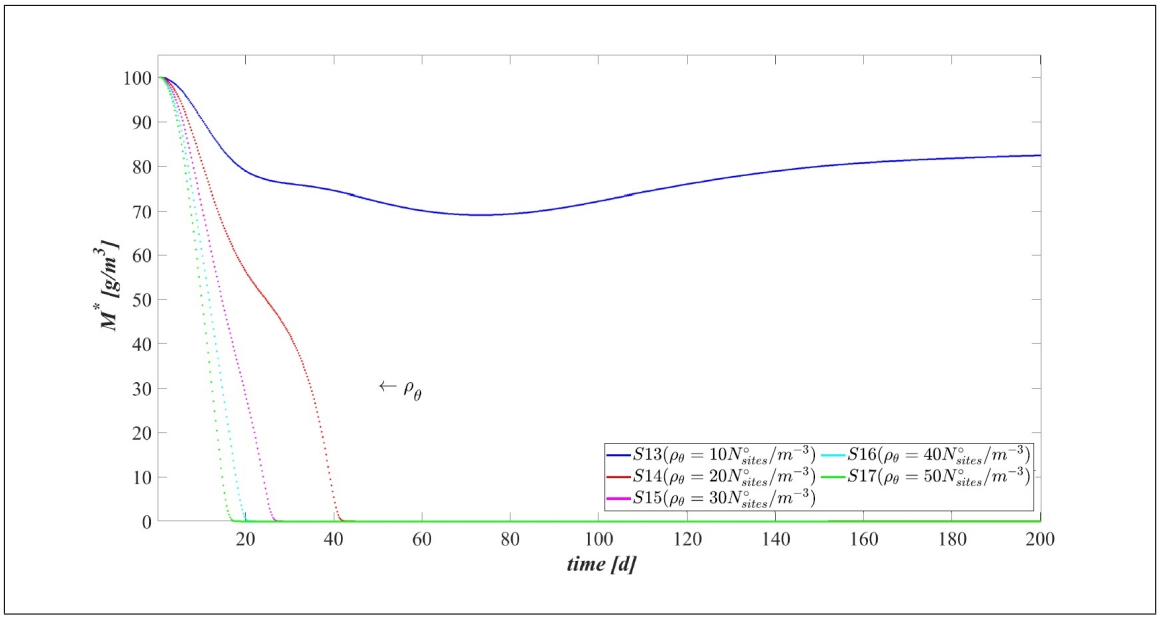


FIGURE 18. *SET*3 - Evolution of metal concentration within the reactor for different densities of binding sites ρ_θ. Wastewater influent composition: $S^{in}_{IC} = 180\ g\ m^{-3}$ (inorganic carbon), $S^{in}_{DOC} = 500\ g\ m^{-3}$ (organic carbon), $S^{in}_{NH_3} = 50\ g\ m^{-3}$ (ammonia), $S^{in}_{NO_3} = 0$ (nitrate), $S^{in}_{O_2} = 0$ (oxygen). $S13$: $\rho_\theta = 10\ N^\circ_{sites}\ m^{-3}$, $S14 : \rho_\theta = 20\ N^\circ_{sites}\ m^{-3}$, $S15 : \rho_\theta = 30\ N^\circ_{sites}\ m^{-3}$, $S16 : \rho_\theta = 40\ N^\circ_{sites}\ m^{-3}$, $S17 : \rho_\theta = 50\ N^\circ_{sites}\ m^{-3}$. Incident light intensity: $I_0 = 0.008\ kmol\ m^{-2}\ d^{-1}$. Duration of the cycle: $\tau = 6\ h$. Time of light exposure: $t_{light} = 50\%\ \tau$.

heavy metals, confirming that algal biomass could efficiently remove them through intracellular accumulation and extracellular immobilization.

- Lastly, the model results show how a higher density of binding sites, induced by heat or acids pretreatments, may enhance the adsorption process and reduce the time required for the complete degradation of substrates and removal of metals [52].

Most of the results shown are qualitatively in accordance with the experimental evidence reported in literature. Accordingly, this model is able to correctly simulate both the formation and maturation of oxygenic photogranules and removal process of toxic metals. From an engineering point of view, this allows to conclude that the model represents a useful tool in studying the removal processes of both organic and inorganic compounds in granular-based sequencing batch reactor systems.

The present work demonstrates the potential applicability of the algal-bacterial granules towards removal of more than one heavy metal. Nevertheless, their joint removal could be not as easy as the removal of a single contaminant. This could be caused by antagonistic effects between the different metals. Looking forward, research activities should be geared towards ways to minimize the antagonistic effects between contaminants.

References

[1] Sarabjeet Singh Ahluwalia and Dinesh Goyal. Microbial and plant derived biomass for removal of heavy metals from wastewater. *Bioresource technology*, 98(12):2243–2257, 2007.

[2] JinShui Yang, Jing Cao, GuanLan Xing, and HongLi Yuan. Lipid production combined with biosorption and bioaccumulation of cadmium, copper, manganese and zinc by oleaginous microalgae chlorella minutissima utex2341. *Bioresource technology*, 175:537–544, 2015.

[3] Katarzyna Chojnacka. Biosorption and bioaccumulation–the prospects for practical applications. *Environment international*, 36(3):299–307, 2010.

[4] Salman H Abbas, Ibrahim M Ismail, Tarek M Mostafa, Abbas H Sulaymon, et al. Biosorption of heavy metals: a review. *J Chem Sci Technol*, 3(4):74–102, 2014.

[5] Marina Fomina and Geoffrey Michael Gadd. Biosorption: current perspectives on concept, definition and application. *Bioresource technology*, 160:3–14, 2014.

[6] Kamra Anjana, Anubha Kaushik, Bala Kiran, and Rani Nisha. Biosorption of cr (vi) by immobilized biomass of two indigenous strains of cyanobacteria isolated from metal contaminated soil. *Journal of Hazardous Materials*, 148(1-2):383–386, 2007.

[7] B D'Acunto, L Frunzo, and MR Mattei. On a free boundary problem for biosorption in biofilms. *Nonlinear Analysis: Real World Applications*, 39:120–141, 2018.

[8] Geoffrey Michael Gadd. Biosorption: critical review of scientific rationale, environmental importance and significance for pollution treatment. *Journal of Chemical Technology & Biotechnology: International Research in Process, Environmental & Clean Technology*, 84(1):13–28, 2009.

[9] Stefano Papirio, Luigi Frunzo, Maria Rosaria Mattei, Alberto Ferraro, Marco Race, Berardino D'Acunto, Francesco Pirozzi, and Giovanni Esposito. Heavy metal removal from wastewaters by biosorption: mechanisms and modeling. In *Sustainable heavy metal remediation*, pages 25–63. Springer, 2017.

[10] Donghee Park, Yeoung-Sang Yun, and Jong Moon Park. The past, present, and future trends of biosorption. *Biotechnology and Bioprocess Engineering*, 15(1):86–102, 2010.

[11] H-C Flemming and Jost Wingender. Relevance of microbial extracellular polymeric substances (epss)-part i: Structural and ecological aspects. *Water science and technology*, 43(6):1–8, 2001.

[12] S Comte, Gilles Guibaud, and Michel Baudu. Biosorption properties of extracellular polymeric substances (eps) towards cd, cu and pb for different ph values. *Journal of hazardous materials*, 151(1):185–193, 2008.

[13] Hong Liu and Herbert HP Fang. Characterization of electrostatic binding sites of extracellular polymers by linear programming analysis of titration data. *Biotechnology and bioengineering*, 80(7):806–811, 2002.

[14] Raul Muñoz, Maria Teresa Alvarez, Adriana Muñoz, Enrique Terrazas, Benoit Guieysse, and Bo Mattiasson. Sequential removal of heavy metals ions and organic pollutants using an algal-bacterial consortium. *Chemosphere*, 63(6):903–911, 2006.

[15] Abeera A Ansari, Ahmed S Abouhend, and Chul Park. Effects of seeding density on photogranulation and the start-up of the oxygenic photogranule process for aeration-free wastewater treatment. *Algal Research*, 40:101495, 2019.

[16] Ahmed S Abouhend, Kim Milferstedt, Jérôme Hamelin, Abeera A Ansari, Caitlyn Butler, Blanca I Carbajal-González, and Chul Park. Growth progression of oxygenic photogranules and its impact on bioactivity for aeration-free wastewater treatment. *Environmental science & technology*, 54(1):486–496, 2019.

[17] Timothy O Ajiboye, Opeyemi A Oyewo, and Damian C Onwudiwe. Simultaneous removal of organics and heavy metals from industrial wastewater: A review. *Chemosphere*, 262:128379, 2021.

[18] Xiaojing Yang, Ziwen Zhao, Yang Yu, Kazuya Shimizu, Zhenya Zhang, Zhongfang Lei, and Duu-Jong Lee. Enhanced biosorption of cr (vi) from synthetic wastewater using algal-bacterial aerobic granular sludge: Batch experiments, kinetics and mechanisms. *Separation and Purification Technology*, 251:117323, 2020.

[19] Xiaojing Yang, Ziwen Zhao, Guanghao Zhang, Shota Hirayama, Bach Van Nguyen, Zhongfang Lei, Kazuya Shimizu, and Zhenya Zhang. Insight into cr (vi) biosorption onto algal-bacterial granular sludge: Cr (vi) bioreduction and its intracellular accumulation in addition to the effects of environmental factors. *Journal of Hazardous Materials*, 414:125479, 2021.

[20] Kim Milferstedt, W Camilla Kuo-Dahab, Caitlyn S Butler, Jérôme Hamelin, Ahmed S Abouhend, Kristie Stauch-White, Adam McNair, Christopher Watt, Blanca I Carbajal-González, Sona Dolan, et al. The importance of filamentous cyanobacteria in the development of oxygenic photogranules. *Scientific reports*, 7(1):1–15, 2017.

[21] A Tenore, MR Mattei, and L Frunzo. Multiscale modelling of oxygenic photogranules. *arXiv preprint arXiv:2104.12273*, 2021.

[22] Alma Mašić and Hermann J Eberl. Persistence in a single species cstr model with suspended flocs and wall attached biofilms. *Bulletin of mathematical biology*, 74(4):1001–1026, 2012.

[23] Alma Mašić and Hermann J Eberl. A modeling and simulation study of the role of suspended microbial populations in nitrification in a biofilm reactor. *Bulletin of mathematical biology*, 76(1):27–58, 2014.

[24] A Tenore, F Russo, MR Mattei, B D'Acunto, G Collins, and L Frunzo. Multiscale modelling of de novo anaerobic granulation. *Bulletin of Mathematical Biology*, 83, 2021.

[25] B D'Acunto, L Frunzo, V Luongo, and MR Mattei. Free boundary approach for the attachment in the initial phase of multispecies biofilm growth. *Zeitschrift für angewandte Mathematik und Physik*, 70(3):1–16, 2019.

[26] B D'Acunto, L Frunzo, V Luongo, MR Mattei, and A Tenore. Free boundary problem for the role of planktonic cells in biofilm formation and development. *Zeitschrift für angewandte Mathematik und Physik*, 72(4):1–17, 2021.

[27] Ahmed S Abouhend, Adam McNair, Wenye C Kuo-Dahab, Christopher Watt, Caitlyn S Butler, Kim Milferstedt, Jérôme Hamelin, Jeongmi Seo, Gitau J Gikonyo, Khalid M El-Moselhy, et al. The oxygenic photogranule process for aeration-free wastewater treatment. *Environmental science & technology*, 52(6):3503–3511, 2018.

[28] Sadiq Naveed, Chonghua Li, Xinda Lu, Shuangshuang Chen, Bin Yin, Chunhua Zhang, and Ying Ge. Microalgal extracellular polymeric substances and their interactions with metal (loid) s: A review. *Critical Reviews in Environmental Science and Technology*, 49(19):1769–1802, 2019.

[29] Kazi A Rahman, Rangarajan Sudarsan, and Hermann J Eberl. A mixed-culture biofilm model with cross-diffusion. *Bulletin of mathematical biology*, 77(11):2086–2124, 2015.

[30] Oskar Wanner and Willi Gujer. A multispecies biofilm model. *Biotechnology and bioengineering*, 28(3):314–328, 1986.

[31] Fazal Abbas, Rangarajan Sudarsan, and Hermann J Eberl. Longtime behavior of one-dimensional biofilm models with shear dependent detachment rates. *Mathematical Biosciences & Engineering*, 9(2):215, 2012.

[32] Cécile Rollet, Laurent Gal, and Jean Guzzo. Biofilm-detached cells, a transition from a sessile to a planktonic phenotype: a comparative study of adhesion and physiological characteristics in pseudomonas aeruginosa. *FEMS microbiology letters*, 290(2):135–142, 2009.

[33] Mercedes Berlanga, Òscar Domènech, and Ricardo Guerrero. Biofilm formation on polystyrene in detached vs. planktonic cells of polyhydroxyalkanoate-accumulating halomonas venusta. *Int Microbiol*, 17:205–212, 2014.

[34] Kendra P Rumbaugh and Karin Sauer. Biofilm dispersion. *Nature Reviews Microbiology*, 18(10):571–586, 2020.

[35] Roberta Ferrentino, Alberto Ferraro, Maria Rosaria Mattei, Giovanni Esposito, and Gianni Andreottola. Process performance optimization and mathematical modelling of a sbr-mbbr treatment at low oxygen concentration. *Process Biochemistry*, 75:230–239, 2018.

[36] Gundula Wolf, Cristian Picioreanu, and Mark CM van Loosdrecht. Kinetic modeling of phototrophic biofilms: the phobia model. *Biotechnology and bioengineering*, 97(5):1064–1079, 2007.

[37] Rajbir Singh, Debarati Paul, and Rakesh K Jain. Biofilms: implications in bioremediation. *Trends in microbiology*, 14(9):389–397, 2006.

[38] SK Mehta and JP Gaur. Use of algae for removing heavy metal ions from wastewater: progress and prospects. *Critical reviews in biotechnology*, 25(3):113–152, 2005.

[39] Joe J Harrison, Howard Ceri, and Raymond J Turner. Multimetal resistance and tolerance in microbial biofilms. *Nature Reviews Microbiology*, 5(12):928–938, 2007.

[40] M Johncy Rani, B Hemambika, J Hemapriya, and V Rajesh Kannan. Comparative assessment of heavy metal removal by immobilized and dead bacterial cells: a biosorption approach. *African Journal of Environmental Science and Technology*, 4(2), 2010.

[41] A Tenore, MR Mattei, and L Frunzo. Modelling the ecology of phototrophic-heterotrophic biofilms. *Communications in Nonlinear Science and Numerical Simulation*, 94:105577, 2021.

[42] Stephen P Long, S Humphries, and Paul G Falkowski. Photoinhibition of photosynthesis in nature. *Annual review of plant biology*, 45(1):633–662, 1994.

[43] John H Steele. Environmental control of photosynthesis in the sea. *Limnology and oceanography*, 7(2):137–150, 1962.

[44] JD Muñoz Sierra, C Picioreanu, and MCM Van Loosdrecht. Modeling phototrophic biofilms in a plug-flow reactor. *Water science and technology*, 70(7):1261–1270, 2014.

[45] Mogens Henze, Willi Gujer, Takashi Mino, and Mark CM van Loosdrecht. *Activated sludge models ASM1, ASM2, ASM2d and ASM3*. IWA publishing, 2000.

[46] Tong Li, Björn Podola, and Michael Melkonian. Investigating dynamic processes in a porous substrate biofilm photobioreactor-a modeling approach. *Algal research*, 13:30–40, 2016.

[47] Brian V Merkey, Bruce E Rittmann, and David L Chopp. Modeling how soluble microbial products (smp) support heterotrophic bacteria in autotroph-based biofilms. *Journal of theoretical biology*, 259(4):670–683, 2009.

[48] Joseph RV Flora, Makram T Suidan, Pratim Biswas, and Gregory D Sayles. Modeling algal biofilms: role of carbon, light, cell surface charge, and ionic species. *Water Environment Research*, 67(1):87–94, 1995.

[49] B D'Acunto, Giovanni Esposito, L Frunzo, MR Mattei, and F Pirozzi. Mathematical modeling of heavy metal biosorption in multispecies biofilms. *Journal of Environmental Engineering*, 142(9):C4015020, 2016.

[50] Berardino D'Acunto and Luigi Frunzo. Qualitative analysis and simulations of a free boundary problem for multispecies biofilm models. *Mathematical and computer modelling*, 53(9-10):1596–1606, 2011.

[51] Doris Brockmann, Yves Gérand, Chul Park, Kim Milferstedt, Arnaud Hélias, and Jérôme Hamelin. Wastewater treatment using oxygenic photogranule-based process has lower environmental impact than conventional activated sludge process. *Bioresource Technology*, 319:124204, 2021.

[52] N Ahalya, TV Ramachandra, and RD Kanamadi. Biosorption of heavy metals. *Res. J. Chem. Environ*, 7(4):71–79, 2003.